Interpreting Wind Directions from Sand Dune Morphologies in the Northern Mid-Latitudes of Mars

April 25, 2019

Jacob Widmer

Advisors: Karen Prestegaard (UMD), Michael Evans (UMD), Lori Fenton (SETI Institute)

University of Maryland Department of Geology Senior Thesis Proposal (GEOL394)

#### **ABSTRACT**

Wind and ice are currently hypothesized to be the two major factors actively shaping the martian surface. Few in-situ measurements exist for near-surface martian wind directions except those collected by several landers and rovers. These measurements are all constrained to localized regions and are unable to accurately depict wind directions and strengths across regional or global scales. However, previous works have used indirect methods such as modeling and surface morphological feature interpretations to infer wind directions in the North Polar Region and Southern Hemisphere. Work has been conducted in the northern mid-latitude region (MLR) of Mars, defined here as 30°-65° N, where dune fields are smaller in size and number compared to the North Polar Region and Southern Hemisphere. As a result, most dune studies conducted at regional and global scales have overlooked the MLR.

This study compares the results of inferred wind directions and their relative sand transporting capability against wind directions from atmospheric modeling in order to determine if there is a significant difference in prevailing wind directions at five dune fields in the Chryse Planitia region of Mars in the present-day martian climate. Only one of the five sites studied was found to have inferred wind directions that were not significantly different from the modeled wind directions. These results provide the opportunity to better understand present-day wind directions as well as ground-truthing results from a climate model and a glimpse into martian weather patterns.

# **Table of Contents**

1.	Introduction and MotivationsPg. 4
2.	BackgroundPg. 5
3.	FrameworkPg. 8
4.	MethodsPg. 9
5.	ResultsPg. 21
6.	DiscussionPg. 30
7.	AcknowledgementsPg. 32
8.	ReferencesPg. 32

#### 1. INTRODUCTION AND MOTIVATIONS

Sand dune fields have been identified throughout the solar system and sit at the boundary between an atmosphere and surface making them uniquely suited for studying weather and climates on planetary bodies beyond Earth. Since the 1940's sand dunes (and collectively, dune fields) have been studied to learn more about wind directions and flow, ultimately providing insight into climate and weather patterns. With the rise of technology over the past 30 years, we've been able to put a handful of instruments on moons and other planets capable of studying the same science. Just like on Earth, knowledge of winds on other planets has been used to keep robotic rovers and landers safe so more information about other worlds can be learned and eventually used as human exploration of other worlds becomes a reality.

For Mars in particular, studies of winds have influenced our understanding of current weather patterns, past climate histories, the sedimentary record, and even Earth through analog studies in comparative planetology, a discipline of planetary science in which similar surface features or phenomena are compared from one planet to another. Understanding wind patterns in relation to martian weather can help operators in mission control stations protect rovers and landers from severe dust storms similar to the storm last summer which resulted in the loss of the rover Opportunity. Using hi-resolution images to study sand dunes, as they are capable of recording pieces of the sedimentary record, can provide a better understanding of the sedimentary record itself as well as inferences to the type of climate in which deposition occurred. Martian wind studies are also important for understanding how the atmosphere interacts with surface features such as craters, as process that has also been studied on Earth. As useful as it would be to know how the winds on Mars interact with the surface, we surprisingly have little data from in-situ measurements on the martian surface. Only a handful of landers and rovers that have survived impacting with the surface have been able to provide this important data. Therefore, a different method is needed if we are to learn more about martian winds.

This investigation aims to provide new insight into martian winds through the use of dunes as a proxy for in-situ measurements which can be widely observed over the surface. This work differs from previous studies in that it:

- 1) Only targets dune fields in the northern mid latitude region, are area of Mars that has been neglected by global dune field surveys (Widmer and Diniega 2018)
- 2) Employs the use of bedform instability mode, a process to calculate potential wind directions, on sand dunes within craters
- 3) And provides a methodology which is capable of being implemented to determine wind directions on a regional or global scale (although only a test region is presented here)

The specific set of hypotheses (null and scientific working) to be tested in this investigation are:

 $H_0$ : Wind directions in the MLR interpreted from dune crest orientation data obtained from remote sensing images are not significantly different from prevailing wind directions generated from the Ames General Circulation Model for Mars.

*Scientific Working:* Wind directions interpolated from dune crest orientation data obtained from remote sensing images are significantly different from prevailing wind directions generated from the Ames General Circulation Model and may represent mean and storm directions

# 2. BACKGROUND

Sand dunes are common to the deserts of Earth but are perhaps even more prominent among other planetary bodies (McKee 1979). Sand dunes have been seen throughout the solar system on Venus, Earth, Mars, Titan, and Pluto (Diniega et al. 2017). But arguably the most impressive display of sand dunes is on Mars where the majority of the surface is covered by sand or dust. The southern hemisphere is characterized by high elevations and old, cratered topography. The northern hemisphere is mostly smooth plains which occur at considerably lower elevations (then the southern hemisphere) and contain the largest sand dune field in the solar system, the North Polar Erg.

# 2.1 Martian Dune Studies

One of the most influential studies for martian dune fields involved the creation of the Mars Global Digital Dune Database (MGD3) (Hayward et al. 2007). The MGD3 provides a record of dune field locations, shape files, and field characteristics for dune fields greater than 1 km² in area. In 2014 an update to the MGD3 was published that estimated martian dunes cover a global total of ~975,000 km² of the planet (Hayward et al. 2014). To aid in cataloging the types of dunes present in each field, the MGD3 provided a definition for each dune type, a system adapted from dune types found on Earth presented by McKee (1979). Figure 1 is an adaptation of Figure 2 from Hayward et al. (2007) and displays several of the most common dune types found on Mars.

On March 10, 2006 NASA's Mars Reconnaissance Orbiter (MRO) reached Mars with a suite of new instruments capable of imaging the martian surface with the highest resolution to date (Zurek and Smrekar 2007). Onboard MRO are the High Resolution Imaging Science Experiment (HiRISE) and Context (CTX) cameras (McEwen et al. 2007, Malin et al. 2007). With these high resolution instruments, direct evidence of sand motion by means of dune migration and sand ripple movement could be imaged (Bridges et al. 2012).

Sand dune fields are useful for a variety of atmospheric and geological inquires as they sit at the boundary between the two fields. Additionally, the large surface area covered by sand dunes provides potential locations to study at nearly any latitude or longitude. Many of the martian dune fields are active under present day conditions which makes them ideal candidates to study in order to learn more about any processes that may be currently acting on the fields (Bridges et al. 2012, Fenton and Hayward 2010).

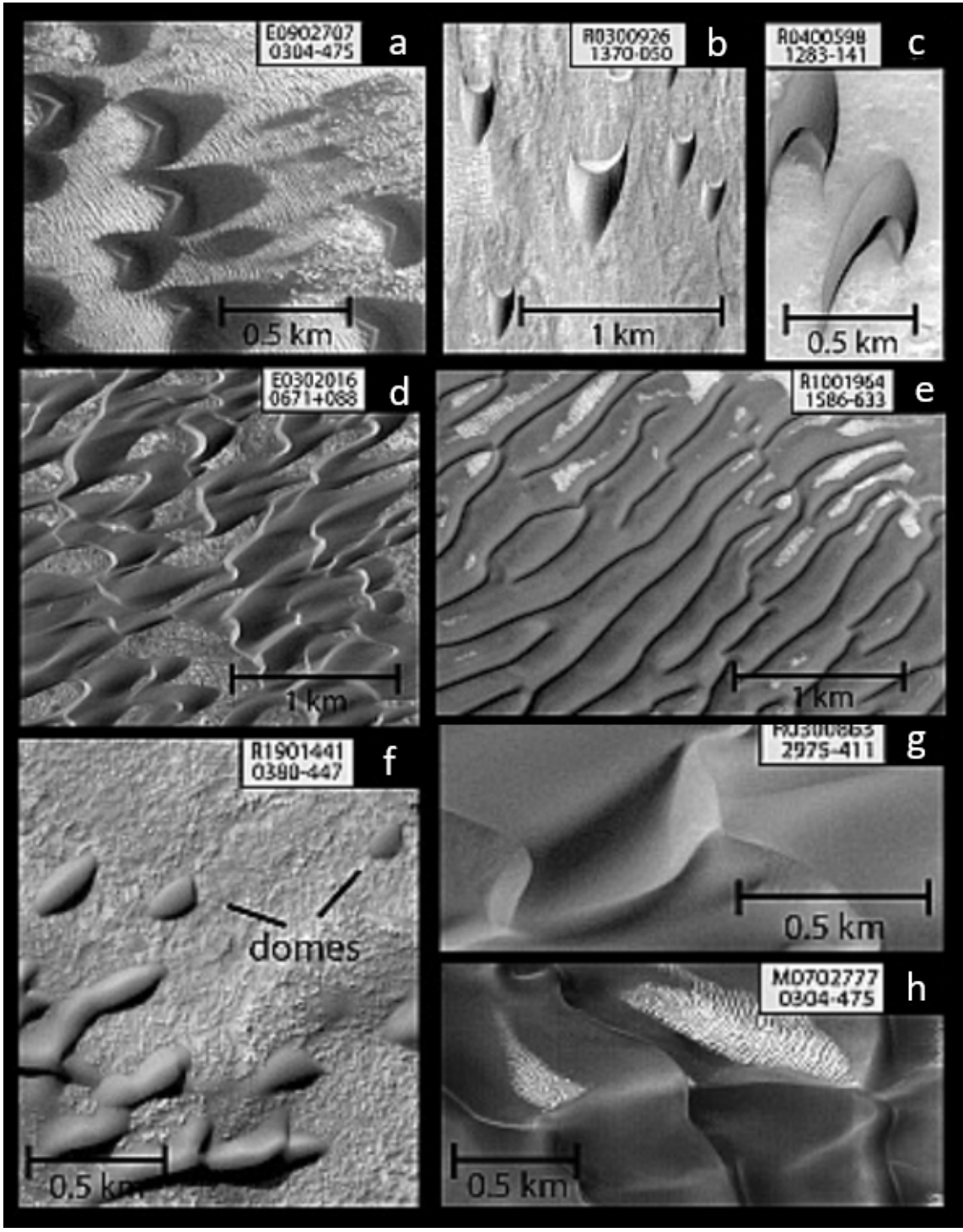


**Figure 1:** An adaptation of Figure 2 from Hayward et al. (2007) showing (a-c) barchan dunes, (d) barchanoid dunes, (e) transverse dunes, (f) dome dunes, and (g-h) star dunes.

### 2.2 Inferred Wind Studies for Mars

Currently, two modes exist that are capable of inferring wind directions from the morphologies of sand dunes. The bedform instability mode (Rubin and Hunter 1987) occurs when a dune field has a high abundance of sand while the fingering mode (Courrech du Pont et al. 2014) occurs when a low amount of sediment is available for dune building.

# 2.2.1 Bedform Instability Mode of Sediment Transport

Experiments initially conducted by Rubin and Hunter (1987) with sand tables and varying directions of winds provided the foundation of the bedform instability mode. By varying the angle between two winds and the amount of sand being transported Rubin and Hunter discovered that several different types of dunes could be constructed. Flume experiments conducted by Rubin and Ikeda (1990) continued to investigate the concept of dune bedform alignment with respect to two wind directions. Dunes produced by the flume experiments followed the same patterns as those seen in Rubin and Hunter (1987).

More recently, Fenton et al. (2014 a and b) conducted a two-part study, first using the bedform instability mode at the Great White Sand Dunes in Colorado, United States in conjunction with several portable meteorological stations. Wind directions inferred through the rule of maximum gross-bedform normal transport (MGBNT) and its inverse (IMGBNT) were able to produce inferred wind directions and dune types similar those recorded and seen in the field (Fenton 2014a). The second study applied the same rules to a dune field in Ganges Chasma, Mars using high-resolution orbital observations from the CTX camera to a mesoscale atmospheric model called MRAMS (Fenton 2014b). This study found that the inferred winds predicted by MGBNT and IMGBNT agreed with the atmospheric model (Fenton 2014b).

### 2.2.2 Fingering Mode of Sediment Transport

Similar to the previous section, the fingering mode began with a need to understand the organization of dune bedform alignment in relation to complex wind regimes on Earth (Reffet et al. 2010). Through a series of experiments and simulations a relationship was discovered relating sand supply to the bedform alignment and the direction of the wind. Later work by Courrech du Pont et al. (2014) developed a model based around the idea of dune orientation and the connection to sediment supply. This model was applied to several of Earth's deserts and found to predict the same types of dunes and similar dune patterns as those seen in the field (Courrech du Pont et al. 2014).

# 2.3 Global and Mesoscale Circulation Models for Mars

Due to a lack of in-situ measurements on the martian surface, models can be a great tool to display an output of a process that's thought to be understood and compare the result with observations. Atmospheric models in particular have been frequently used to assess wind directions in dune fields at global scales (Gardin et al. 2012, Hayward et al. 2007, 2009, 2014). Studies that include mesoscale modelling of winds in dune fields include Fenton et al. (2014b) and Hayward et al. (2009).

### 3 FRAMEWORK

# 3.1 Project overview

Conceptually, the best way to understand martian wind regimes would be to measure wind velocities at the surface in many different locations over an extended period of time. Since these measurements do not currently exist with the spatial or temporal distribution needed, other options from currently available datasets are needed to determine surface wind circulation patterns. This study can be separated into three components: 1) measurements and calculations from orbital images of sand dunes 2) calculations of resulting wind patterns from an atmospheric global circulation model and 3) the analysis of the results from component 1) and 2). The landforms to be measured, specifically sand dunes, will act as proxy in-situ measurements while the model will represent the current state of knowledge of for the planet's atmospheric processes. Figure 2 shows a simplified flow chart of how the three components come together to produce wind directions at a single study site. In Figure 2 component 1) is represented by the purple boxes, 2) by the green boxes, and 3) by the blue boxes.

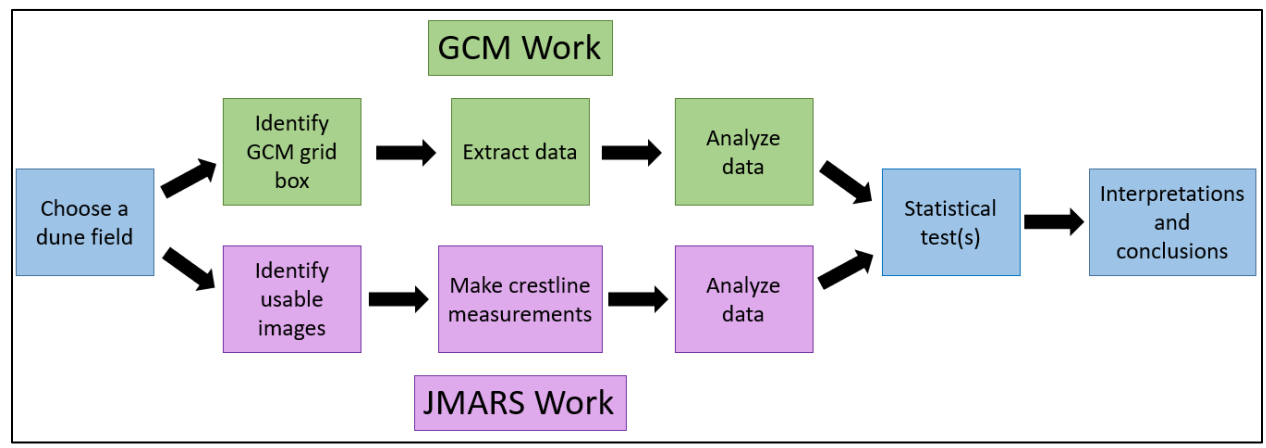
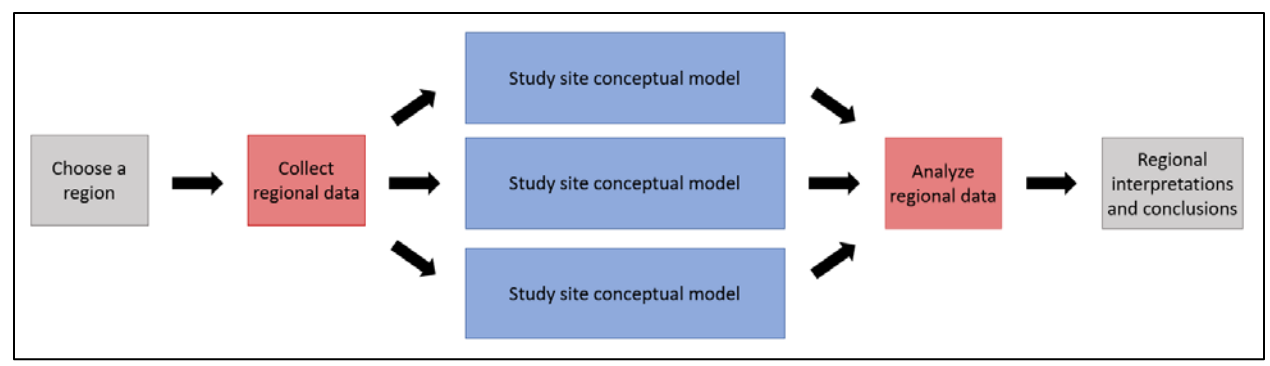


Figure 2: Study site conceptual model indicating how components 1)-3) combine.

The three components were created with the intention of a modular-type design, meaning they could be flexible in terms of planning various steps in the project's progression. This design also allowed for several sites to be investigated at once. With work at each site capable of progressing at various stages of completion, some degree of setbacks or roadblocks could be accounted for so the project could continue to progress. In addition to the modular design, the project was designed to run as a series of research cycles with the completion of components 1) -3) at several dune fields in a single geographic region to equate to a full research cycle. At the end of one research cycle, several study sites would be chosen in a new geographic region and the process would start over again. A flowchart depicting the integrated process between components and research cycles is shown in Figure 3. Note that each rectangular blue box in Figure 3 contains the entire model of Figure 2.



**Figure 3:** Model of the research cycle designed for studying inferred winds at dune fields on regional to global scales. Note the incorporation of components 1)-3) from Figure 2 as blue, rectangular boxes in this figure.

# 3.2 Project Limitations

The primary purpose of this investigation is to provide insight into martian wind directions via observable landforms on the surface. This is a difficult task which can be further complicated by specific inferences that must be made in order to produce expected wind directions (i.e. not directly observable). This study identifies several types of limitations such as restrictions on high resolution data, useful locations to study, and methods used to infer wind directions.

CTX and HiRISE images best fulfill the resolution required for detailed surface morphology-based investigations. However, both instruments are on board MRO which is only capable of imaging the martian surface in the afternoon (approximately 3-4 pm local Mars time) due to the spacecraft's orbital configuration. Therefore, high resolution images are only collected at one time of day making diurnal variation in the martian wind regime impossible to determine from the proposed methods.

A significant limitation in identifying useful locations to study is the location of the dune fields. The importance of using sand dunes in wind studies was described in *Section 1: Introduction and Motivations* however sand dunes are not uniformly distributed over the martian surface and are preferentially located in topographic lows (many of which are craters). Therefore, the restriction of study sites to areas with sand dunes is a geographical limitation. Inferring wind directions from a variety of geological and metrological features such as dust devil tracks, fan deposits, and cloud movements have been hypothesized but are not evaluated in this work. Additionally, the lack of in-situ measurements of MLR surface winds combined with a lack of information in the current literature on MLR sand dunes will keep the focus of this study in the MLR.

The method used to infer wind directions can also be a limitation and provide an over or under estimation of wind directions if not used properly. As mentioned in *Section 2: Background*, two modes exist for inferring wind directions from sand dune morphologies based on sediment availability in the dune field: 1) Bedform instability mode and 2) Fingering mode. This study will focus on inferring wind directions using the bedform instability mode. However, updates to this study (already in progress) will seek to create a dual-mode methodology.

#### 4 METHODS

This study has included a variety of materials and methods due to the cross disciplinary nature of geomorphic observations and atmospheric modeling. In particular, several important

pieces of this project include the materials used and their justification, the work conducted in the GIS software JMARS, the method of calculating and inferring wind directions, the output from the NASA Ames Mars GCM, and finally the statistical tests used to compare the inferred and modeled winds.

### 4.1 Justification of Materials Used

Since this study is theoretical in nature (i.e. we don't have direct access to Mars for observations or sample collection), all work on this project has required computer access. Additional materials included a Geographic Information System (GIS), high-resolution images of the martian surface, and access to a martian global climate model.

#### 4.1.1 JMARS

The bulk of the work for this investigation has been performed in the Java Mission-Planning and Analysis for Remote Sensing (JMARS) software. JMARS is a free GIS package that is distributed and maintained by the Mars Space Flight Facility at Arizona State University (Christensen et al. 2009). This tool was originally designed to aid in mission planning and data analysis for Mars but has since expanded to encompass information on all of the rocky planets and most of the prominent solid bodies in the solar system.

JMARS is a powerful tool in exploring martian morphology because of its connection to NASA's Planetary Data System (pds.nasa.gov) which acts as a long-term catalog for all of NASA's past missions. This connection allows users to search for and display a variety of mission data, specifically Mars data in this case, within JMARS. The GIS portion of JMARS allows users to create different layers of information, similar to Photoshop, and combine layers together to collect or compare different types of data in a single location. Types of data can include surface images, a variety of maps, user created polygons and measurements, spectral data, and many more.

#### *4.1.2 Images*

Malin System's CTX camera was designed to provide context images for other MRO datasets and investigate a variety of geologic features as part of its own science mission (Malin et al. 2007). CTX currently has ~100% global surface coverage at 4m/ pixel resolution. The HiRISE camera, built by Ball Aerospace and Technologies Corporation, is also onboard MRO and is capable of imaging at 25 cm/ pixel resolution (McEwen et al. 2007). Current global coverage is ~3% but has been a major asset in detecting morphological changes and repeat imaging. The highest resolution of surface images is required to investigate sand dunes to the level of detail need for inferring wind directions. Therefore, CTX and HiRISE images have been chosen for use as base images for the mapping portion of this study.

#### 4.1.3 Ames GCM

Finally, the Ames GCM has been selected for use in this investigation based on developmental history (including past inferred wind studies), model adaptability, and prior connections to the Ames development group. The Ames GCM models the martian atmosphere on a three-dimensional Arakawa C-style point grid (Kahre et al.2006). Data can be collected over a  $5^{\circ}$  latitude by  $6^{\circ}$  longitude area with a maximum surface resolution of  $\sim 10\text{-}20\text{m}$  (Kahre et al. 2006). Model results provide wind direction, wind stress (i.e., strength), and many other

atmospheric characteristics up to 16 times throughout a martian day and up to a period of several mars years (Hayward et al. 2009; Fenton, personal communication).

### **4.2 JMARS**

The JMARS software is a powerful planetary GIS package that combines a suite of planetary datasets with traditional tools for analyzing geospatial data while maintaining the flexibility to upload customized information to suit individual research needs. JMARS was used to select study sites, collect environmental information through various databases, and measure the crestlines of sand dunes.

### 4.2.1 Study Site Selection

In order to identify locations that would be evaluated in this study (i.e. study sites), criteria for study site selection first had to be developed. These criteria were primarily used to eliminate locations where MLR dune fields did not have the necessary image coverage for the investigation. Additional constraints were placed on site selection criteria for the first few dune fields in order to obtain the most ideal study sites for the development of a robust, yet feasible methodology. Study site criteria were:

- "Clustered" dune fields (i.e. high spatial density in a small region)
- Good CTX coverage of the dune field (i.e. at least 1 clear image included ~70-100% coverage of the dune field)
- Good HiRISE coverage (i.e. at least 1 clear image included ~70-100% coverage of the dune field, if possible)
- Simple topography (i.e. no complicated surface features; flat surrounding area)
- Common geologic unit in host environment (if possible)

Using the criteria listed above, six potential Target Regions (TRs) were identified for further evaluation. Figure 4 provides the geographical distribution of the TRs in a subsection of the martian surface, the northern mid latitude region (MLR), defined as 30-65° N. The source of the map is the MOLA 128ppd global colorized elevation map. The six TRs displayed have clusters of dune fields, each of which contains 4-9 individual dune fields. Many additional dune fields exist in the MLR however, most of the remaining fields are not constrained to small localized areas or are positioned in more complex topography.

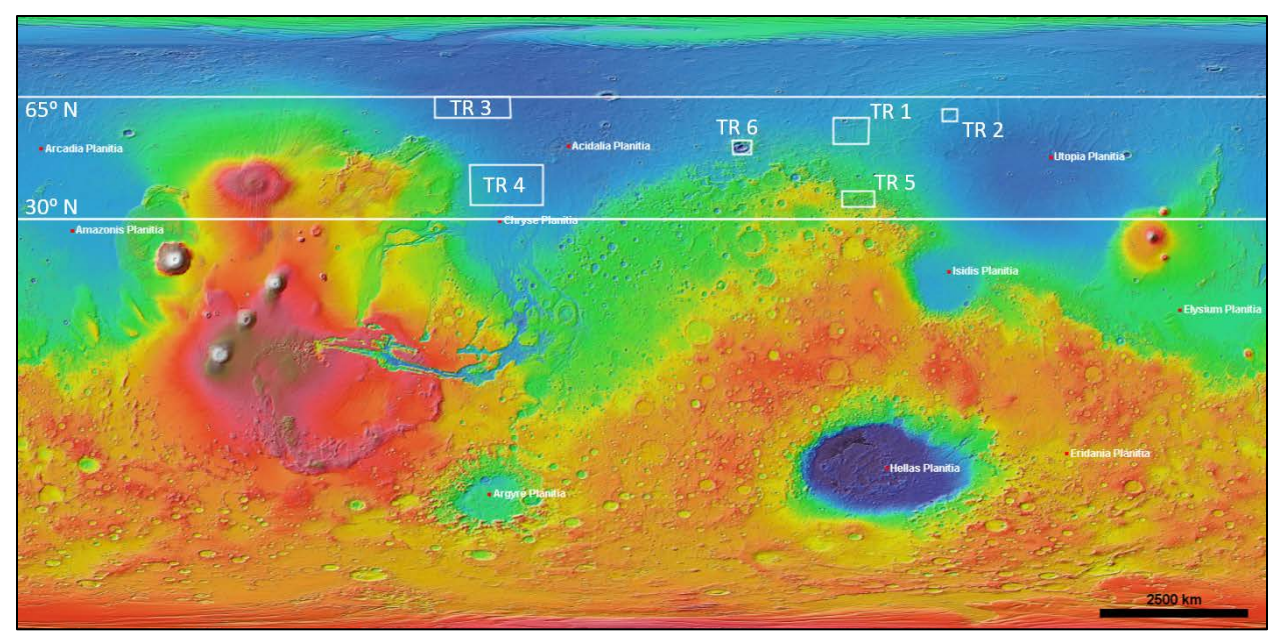


**Figure 4:** Target regions (white boxes) identified for initial region of project study. These 6 regions are located in the Northern Mid-Latitude Region (MLR) and are overlaid on a 128ppd MOLA colorized elevation map where warmer colors indicate higher elevations and cooler colors are at lower elevations.

Of the six TRs identified, TR4 was selected for study during the first cycle of research during the fall semester. This region was chosen as it best satisfied all of the selection criteria, containing nine different dune fields with good image coverage in a simple topographic setting. Of the nine fields located in TR4, five dune fields were chosen for study. The distribution of dune fields in TR4 is shown in Figure 5 with study sites circled in black and characteristics of the craters that host the selected dune fields are listed in Table 1.

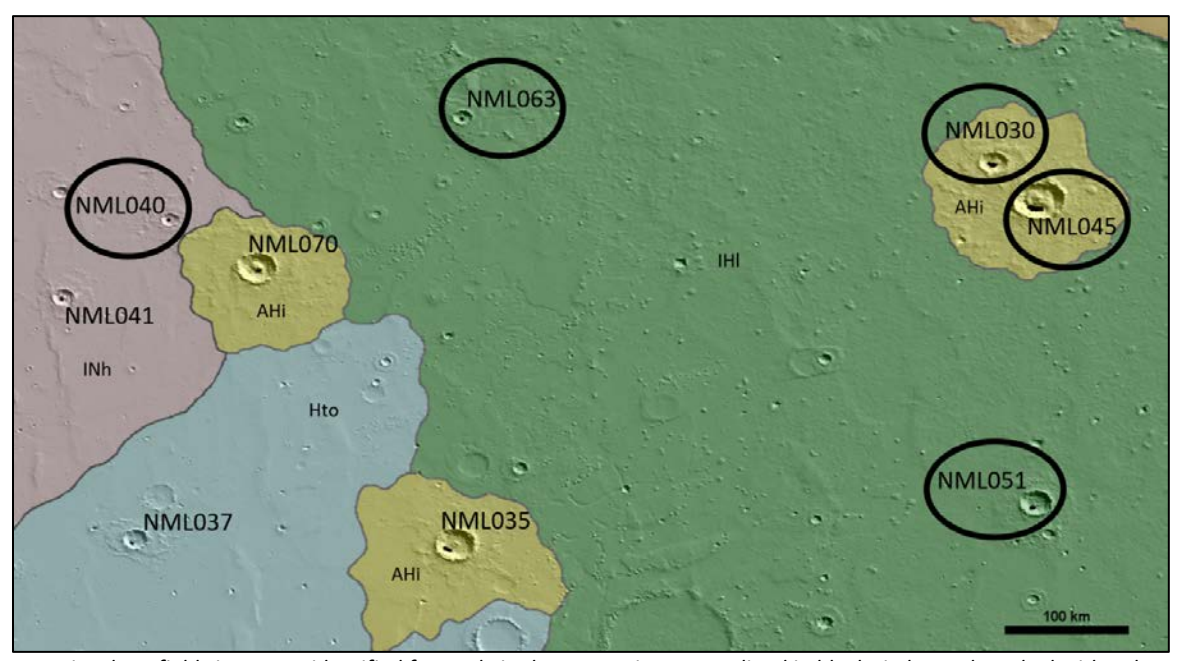


**Figure 5:** Five dune fields in craters identified for study in the TR4 region are outlined in black circles and marked with a dune field ID in the form of Northern Mid-Latitude (NML) XXX. Colored regions represent different geologic deposits based off the USGS geologic map of Mars presented in Tanaka et al. 2014.

Dune Field ID	Center Latitude (N)	Center Longitude (E)	Host Crater Diameter (km)	Maximum Elevation (m)	Minimum Elevation (m)	Crater Depth (m)
NML030	42.620	328.796	22.1	-3999	-5581	1582
NML063	43.432	319.316	14.8	-3603	-4833	1230
NML040	41.627	314.07	13.6	-3507	-4427	920
NML051	36.479	329.509	26.5	-3512	-5523	2011
NML045	42.027	329.608	40.7	-3582	-6009	2427

**Table 1:** Several environmental parameters for the craters that host the selected dune fields are listed in the above table. Crater elevations and depth calculations utilized map sampled MOLA elevation data collected using crater rim outlines from Robbins and Hynek (2012a).

### 4.2.2 Choosing Base Images

There are several parameters that must be considered when choosing base images for high-resolution mapping of sand dunes on Mars. Mars year, solar longitude ( $L_s$ ), and location. Mars year describes the year in martian history an image was taken.  $L_s$  is a measure of where Mars is in its orbit and will have a value between 0-360. Essentially  $L_s$  is a measure of seasonality and in the northern hemisphere an  $L_s$  value of 0-90 corresponds to the spring season, 90-180 is the summer, 180-270 is fall, and 270-360 is winter. Mars year and  $L_s$  are often paired together to describe seasonal processes or significant events in martian history such as large dust storms. Location of image coverage is an obvious but crucial consideration when choosing images.

Ideal images for this study were summertime HiRISE images with variations in coverage over each dune field in the target region. However, due to limited image coverage over most of the mid-latitude dune fields, a tradeoff in temporal verses spatial coverage was made that expanded the actual timing of images used from early spring (L<sub>s</sub> 31) to late summer (L<sub>s</sub> 179). Early spring timing was a concern for seasonal frost which can armor sand dunes preventing crestlines from responding to the most recent wind patterns. All images used were checked for frost and confirmed to be frost free, a finding consistent with the most recent results of mid-latitude seasonal frost observations (Widmer and Diniega 2019).

### *4.2.3 Measuring Dune Crestlines*

Using the JMARS software, high-resolution HiRISE images (and CTX images when HiRISE was unavailable) were rendered in order to identify individual dune crestlines. A custom shape layer was then overlaid on the images where the crestlines were traced by hand. Crestline directions were recorded in degrees (0°-360° clockwise from north) through the line direction function in JMARS and saved for later use. The line direction function in JMARS can only record the direction of a polyline between two points (i.e. straight lines) but to be accurately mapped, nearly every crestline requires a multipoint polyline to account for natural deviations in the dune crests. To combat this issue, two separate mapping types were developed and implemented to obtain accurate crestline directions.

### Type I Measurements

Type 1 measurements refer to straight line measurements which comprise the bulk of the dune crestline measurements. Although a given crestline cannot by modeled by a single polyline segment, the crestline geometry can be deconstructed and approximated with multiple polyline

segments. Each polyline segment records the direction of the crestline's orientation as a specific piece of the entire crestline which can later be combined to obtain the direction of the entire crestline and thus, the dune. An example of this method can be seen in Figure 6 where each color represents a separate polyline and the corresponding direction is color coded to the polyline segment.

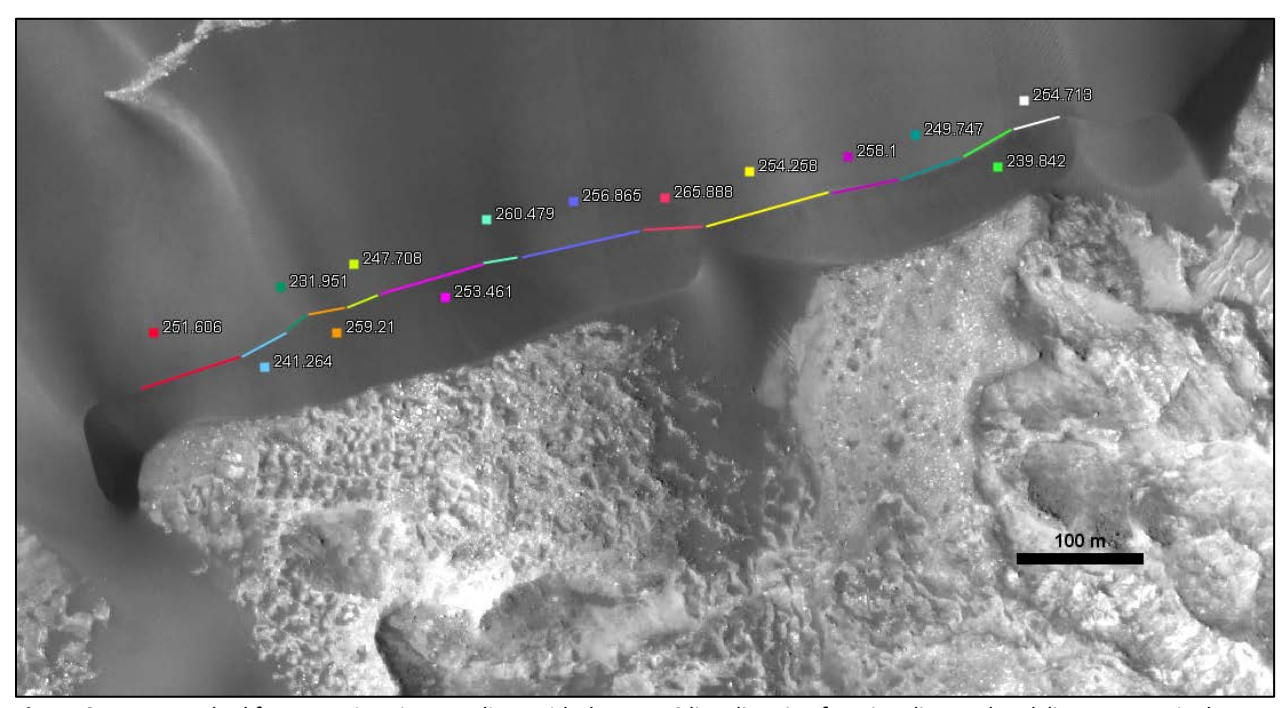


**Figure 6:** A new method for approximating crestlines with the JMARS line direction functionality. Each polyline segment is shown in a different color and the corresponding orientation in degrees (0-360) is color coded to the polyline segment.

# Type II Measurements

Type 2 measurements are used to approximate the direction of crestlines for semicircular features, most notably, individual barchan dunes and barchanoid dunes throughout a dune field. Barchan dunes are known for clearly recording the direction of the unidirectional wind that formed them by advancing in the direction of wind flow or by growing arms which point in the direction of the flow. However, barchanoids are not always formed in a unidirectional wind regime allowing for variations in the classic semicircular geometry characteristic of barchan dunes.

To ensure consistency in the measurements recorded through this technique (shown in Figure 7), a polyline was drawn from one point on a horn to a point on the adjacent horn in order to approximate a semicircular crestline with a apex of the dune located at the center point of the semicircle. If placed at the apex of the dune, the straight line crossing the horns of the barchan dune would be tangential to the apex of the barchan crestline and acts as an estimated crestline approximation. The wind direction responsible for the formation of the barchan dune could then be approximated as the normal (i.e. imaginary line oriented 90° perpendicular) to the polyline. This technique was also used to approximate wind directions for semicircular crestlines of barchanoid dunes interspersed throughout dune fields in the target region.

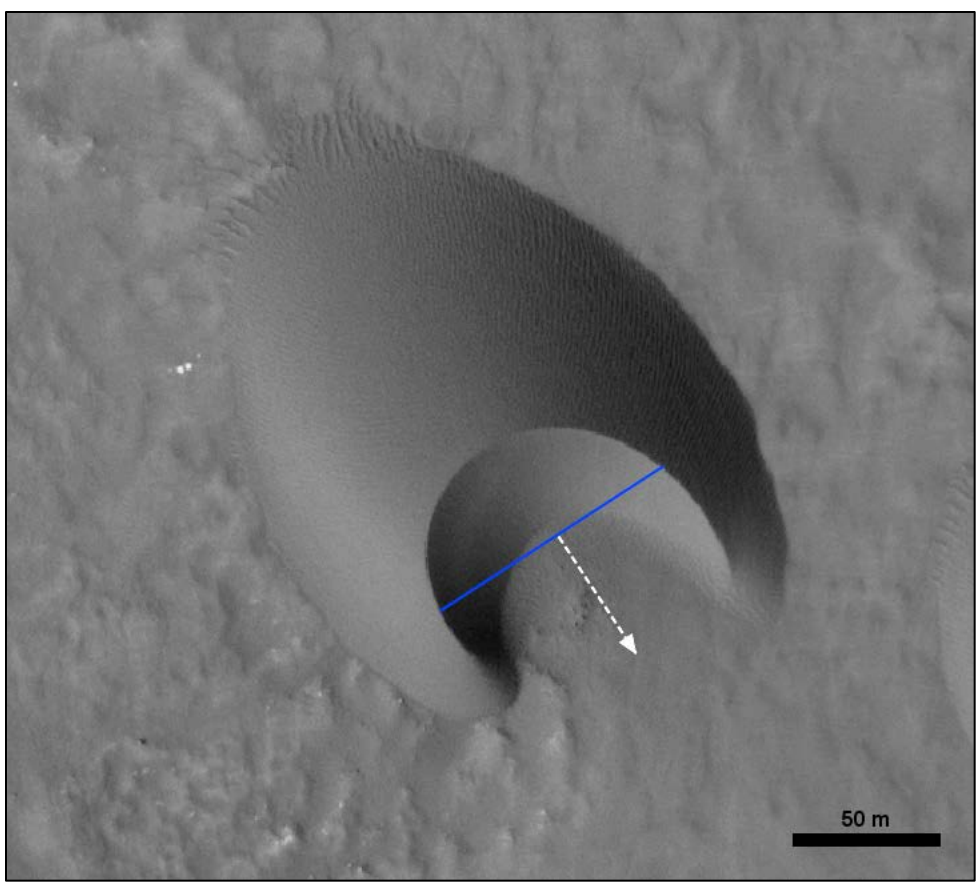


**Figure 7:** An example of a type II measurement used to approximate curved crestlines from individual barchan and barchanoid dunes and other semicircular crestline features. A blue polyline is drawn to approximate a semicircular crestline with the highest point of the dune crest at the midpoint of the semicircular crestline. The blue poyline serves as the crestline for the barchan dune and the white dashed polyline is the normal (perpendicular to the crestline) and indicates the direction of wind flow (top left to bottom right of image).

# 4.2.4 Generating Crestline Groups

A large portion of this study was the analysis needed for creating groups of similarly oriented dune crestlines which are later used to infer wind directions. This analysis involves the separation of individual polyline segments based on a standardized set of crestline coloring rules developed for this project.

# Rules for Crestline Coloring

A method for organizing polylines into different groups was needed for calculating inferred wind directions and recording the number of measurements for statistical analysis later in the study. The easiest way to keep records of the different groups of polylines was to assign each group a different color. Those colors would then indicate all of the crestlines that trended in a similar direction within one dune field. Type I measurement groups followed a pattern: the first set of similar trending polylines were colored orange, the second set was colored pink, the third green and fourth red. Although, not every dune field contained four different sets of type I measurements. Type II measurements were colored in varying shades of blue: the first set of similarly trending polylines were colored dark blue, the second set was light blue, and the third set was a medium-toned sky blue henceforth known simply as blue. It should be noted that many of the dune fields only required one or two sets of type II measurement groups.

Dune crestlines are easy to separate when they appear as individual dunes but become much more difficult to understand when the dune field is confined to a crater where many different wind directions can influence crestlines and force dunes to collide with one another.

To keep mapping simple, two rules were developed to know when to change color from one set of crestlines to another.

- 1) The intersection of three or more crestlines marks a point where crestlines can change colors as they pass from one side of the intersection point to another (see Figure 8a for example).
- 2) Transitions from type I measurements to type II measurements mark boundaries where polyline segments can change colors indicating changes in group directions (see Figure 8b for example)

Coloring of individual crestline segments occurred via visual inspection in the JMARS software and manually changing the color of each segment.

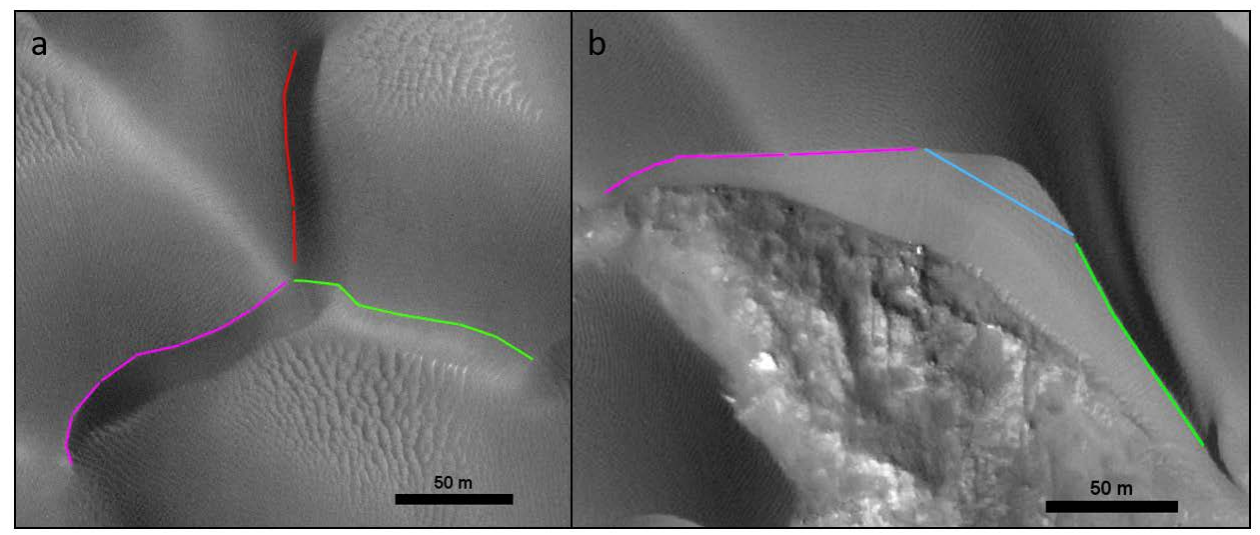


**Figure 8:** Examples of the two rules used for knowing when to change color groups of crestline measurements. (a) Corresponds to rule 1 in the text and (b) corresponds to rule 2.

# 4.2.5 Type I/ II Measurement Uncertainty

Both measurement types are mapped manually in JMARS subjecting them to the same sources of uncertainty. These sources include, but are not limited to, human error, the limit of resolution for the JMARS software, and the resolution of the HiRISE and CTX images used. The maximum resolution for HiRISE and CTX images is 0.25m/ pixel and 4m/ pixel, respectively (McEwen et al. 2007, Malin et al. 2007). This study only requires a CTX level of resolution for feasibility; however, study sites were specifically chosen that had higher resolution HiRISE images for dune crestline mapping. Since the base images used for mapping exceed the required resolution, the uncertainty associated with the base images is negligible compared to the other factors mentioned. Similarly, the JMARS software collects polyline and polygon information on a pixel by pixel scale deeming its associated uncertainty negligible in comparison as well. The largest factor in the uncertainty is human error. In order to determine the level of uncertainty, two sensitivity tests were conducted, one for each of the two measurement types. These tests identified the uncertainty in measurement type I and II directions as 0.95° and 2.8°, respectively.

### 4.3 Ames GCM Output

The Ames GCM is a complex tool, capable of investigating a range of atmospheric parameters such as dust loading, the behavior of radiative clouds, and properties of atmospheric volatiles to name a few. This version of the GCM had been run for a previous study and simulated present-day conditions on Mars (Fenton et al. 2018). The GCM outputs 2 surface wind stress vector components (east-west and north-south) per timestep, 8 timesteps per sol (martian day), and 669 sols per year for a total of 10704 wind directions in any GCM grid box.

Due to its complexity, the output for the model can only be accessed with scripts coded in certain computing languages. Here, two scripts that work sequentially, written in Interactive Data Language (IDL) by Lori Fenton, were used to extract modeled wind directions. The first script  $rd\_ncdf\_case$ , extracts a list of several model parameters from the standard GCM output, such as surface pressure, surface temperature, and wind stresses for each time-step in a designated grid box. Figure 9 shows the GCM grid boxes (green) for the TR4 region (white box) and outlines of the craters containing study sites (black ovals) which were mapped in JMARS (Robbins and Hynek 2012a). The second script,  $ustar\_sandflux$ , ingested the model parameters from  $rd\_ncdf\_case$  and ran a series of calculations to produce the modeled wind directions over each time-step. Then a list of wind directions for a single grid box could be saved to an external file for analysis.

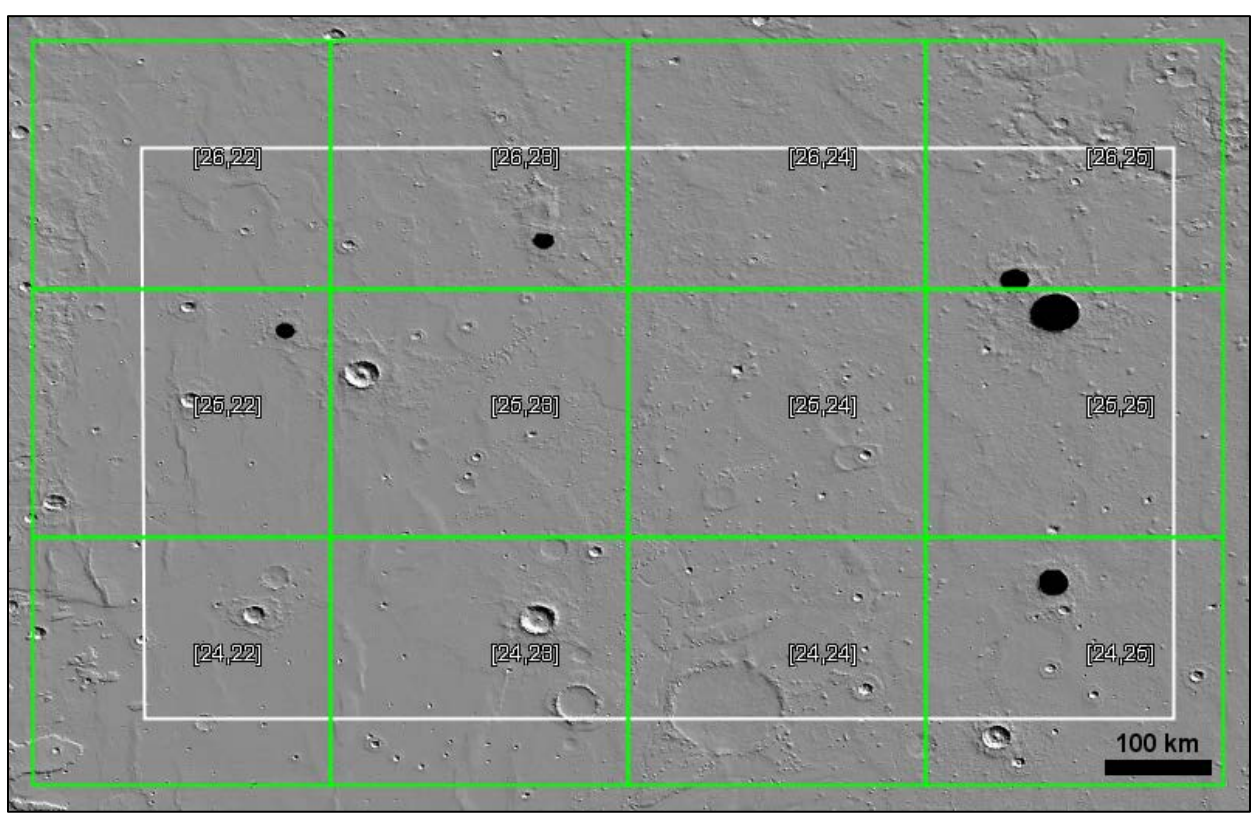


**Figure 9:** NASA's Ames GCM runs on a global grid of 5°x6° resolution. To assist with extracting model output and for reference in location to TR4 (white box) a portion of the GCM grid (green boxes) was created in JMARS with GCM designated latitude and longitude coordinates displayed at the center of each green box. Black ovals from (Robbins and Hynek 2012a) indicate the locations of the craters that host TR4's 9 dune fields.

### 4.3.1 Displaying Modeled Wind Directions

The output for each GCM grid box contains 10,704 wind directions so a qualitative way was needed to view the data in a format other than a list of numerical values in order to understand how the model winds were distributed. A rose histogram was created for the output of each of the five grid boxes to display the modeled wind directions. Modeled winds stresses were not filtered for saltation strength because 1) not enough information is known about the value of wind stress required to activate saltation (S<sub>a</sub>) on Mars and 2) there is no way to account for the winds below S<sub>a</sub> value that participate in saltation of grains that have already begun moving in saltation (Fenton, personal communication). Data was binned at 10° intervals and circles with increasing diameters marked the number of counts in each 10° bin. To maintain consistency with the plots created through the IMGBNT calculations, the rose histograms display the upwind direction of the modeled winds (i.e. direction the winds are entering the dune fields).

### **4.4 Statistical Test(s)**

Once data have been collected from dune field measurements and the GCM output, they are compared to determine if their mean directions are significantly different. In order to choose an appropriate statistical model for this comparison, normality of the data first needed to be assessed. A review of the data through a series of histograms indicated that the dune field measurements were all normally distributed however, the data from the GCM were slightly variable between being normally distributed and slightly non-normally distributed. Due to time constraints the data from the GCM was assessed as normally distributed. Potential consequences of this assignment of normality are presented in the discussion section. The statistical model chosen to best compare these two normally distributed, independent datasets was a T-Test.

### 4.4.1 Calculating Type I Measurement Statistical Values

Type I measurements approximate straight dune crestlines as a collection of polyline segments, each recording their directional orientation. Each group of type I measurements, previously identified and color coded, was used to obtain a mean crestline direction by using a weighted mean, shown in Eq. 1, of all measurements in a given color group. Here  $\theta_A$  is the weighted mean crestline orientation in degrees (0°-360°),  $\theta_i$  is the direction of the i<sup>th</sup> polyline segment in the group, and  $s_i$  is the length of the i<sup>th</sup> polyline segment in the group. Variation in the weighted mean was calculated using the 'stdey' function in Microsoft Office's Excel program.

$$\theta_A = \frac{\sum_{i=1}^n \theta_i s_i}{\sum_{i=1}^n s_i}$$
 Eq. 1

### 4.4.2 Calculating Type II Measurement Statistical Values

Each group of type II measurements represents a collection of crestline approximations for semicircular crestline features. Type II measurements are handled differently as their semicircular structures are assumed to indicate specific inferred wind directions. Adding a line normal to the crestline approximation will provide the inferred wind direction for a given feature in the given type II measurement group (i.e. +90° so downwind direction orientation is perpendicular to approximated crestline).

When all of the crestline normals have been applied to a type II group, the mean of all the normal values in the group can be taken to provide a mean inferred wind direction for that group. Wind directions are measured on angular scales and any statistical function for those directions

needs to be evaluated on an angular scale instead of a linear one (Berens 2009). To find the mean of the type II groups, a circular statistics toolbox called CircStat was used in conjunction with Mathworks Matlab software (Berens 2009). Each group of type II measurement inferred winds were written into variables in a matlab script and run through CircStat's 'circ\_mean(x)' function to calculate the mean value of each type II group. The 'circ\_mean' function works by converting each point in a data set into a unit vector containing the coordinates of the point on the unit circle (Berens 2009). The unit vectors are averaged to create a single value (the mean) which is then converted back into degrees.

The CircStat toolbox was also used to calculate the variance in the inferred wind directions using the 'circ\_std(x)' function (Berens 2009). This function calculates the angular deviation, as opposed to the circular standard deviation, and is shown in Eq. 2. Here, s is the standard (angular) deviation in a data set and R is the resultant vector length of the data set (Berens 2009).

$$s = \sqrt{2(1-R)}$$
 Eq. 2

### 4.4.3 Calculating Modeled Wind Statistical Values

As previously mentioned, the Ames GCM outputs 10,704 wind directions per grid box. Wind directions for each grid box are saved to output files which are then ingested into the Matlab software for statistical analysis. Similar to the analysis of the type II inferred wind directions, the mean and standard deviation for each set of modeled winds is calculated using the CircStat toolbox 'circ\_mean' and circ\_std functions.

# 4.4.4 Statistical Model for Comparing Inferred and Modeled Winds

The statistical model chosen to test the null hypothesis was a t-test for comparing the means of two independent samples. The null hypothesis for this kind of t-test is that the mean from sample A is equal to the mean of sample B. In order to compute the results for a t-test, three parameters are needed: a critical P value ( $P_{crit}$ ), number of tails, and degrees of freedom (DOF). The  $P_{crit}$  value and number of tails are independent variables and the DOF are dependent on the number of points in a dataset. These three parameters define a critical t value ( $t_{crit}$ ) which can be looked up online or in any statistical textbook. The  $t_{crit}$  value is then compared to t, the value produced from the t-test and determines whether the null hypothesis is accepted or rejected.

$$T = \frac{X_a - X_b}{\sqrt{\frac{S_a^2}{N_a} + \frac{S_b^2}{N_b}}}$$
 Eq. 3

Eq. 3 displays the formula for the T-Test where  $X_a$  is the mean from sample A,  $S_a$  is the standard deviation in sample A, and  $N_a$  is the number of points in sample A. Variables with the subscript b are values taken from sample B. For this study, a  $P_{crit}$  value of 0.2 was chosen to account for a natural deviation in wind directions meaning that the calculated T value is representative of 80% of the results. This model was run as a 2-tailed in order to check the null hypothesis of significant difference however the direction of that difference was not important at the time of testing.

#### 5 RESULTS

Using the methods above, wind directions are inferred from IMGBNT calculations for crestlines in bed instability mode for each of the five dune fields in the target region (TR4) and separated by dune field ID (i.e. NMLXXX). The IMGBNT method assumes two wind directions are responsible for shaping crestlines during the most recent period of dune construction so two inferred wind directions are provided for each dune field. All winds presented (inferred and modeled) are given in the standard meteorological way of the upwind direction (i.e. the direction wind is entering the dune field). Dune morphology for each field was checked and found to be consistent with the IMGBNT assumption that at least two winds were acting on the dunes in each field. Results from the Ames GCM output and statistical tests comparing the inferred and modeled winds are also discussed. Finally, this section concludes with a summary of the work completed and lays the basis for scientific discussion and broader impacts in the following sections.

# 5.1 Dune Field NML030 Inferred Wind Directions

NML030 is located in the north west corner of TR4 with the center of the field at 42.6 N and 328.8 E. A total of 1140 crestlines were mapped in this field and then separated into 6 colored groups: dark blue (type II), light blue (type II), orange (type I), pink (type I), green (type I), and red (type I). Figure 10 displays the resulting colored crestline groups overlaid on a composite image of HiRISE image ESP\_043611\_2230 and CTX image F20\_043611\_2229\_XN\_42N031W. Using the same dune classification scheme provided by Hayward et al. 2007, 5 dune morphologies were identified in NML030: barchan, barchanoid, transverse, dome, and star dunes.

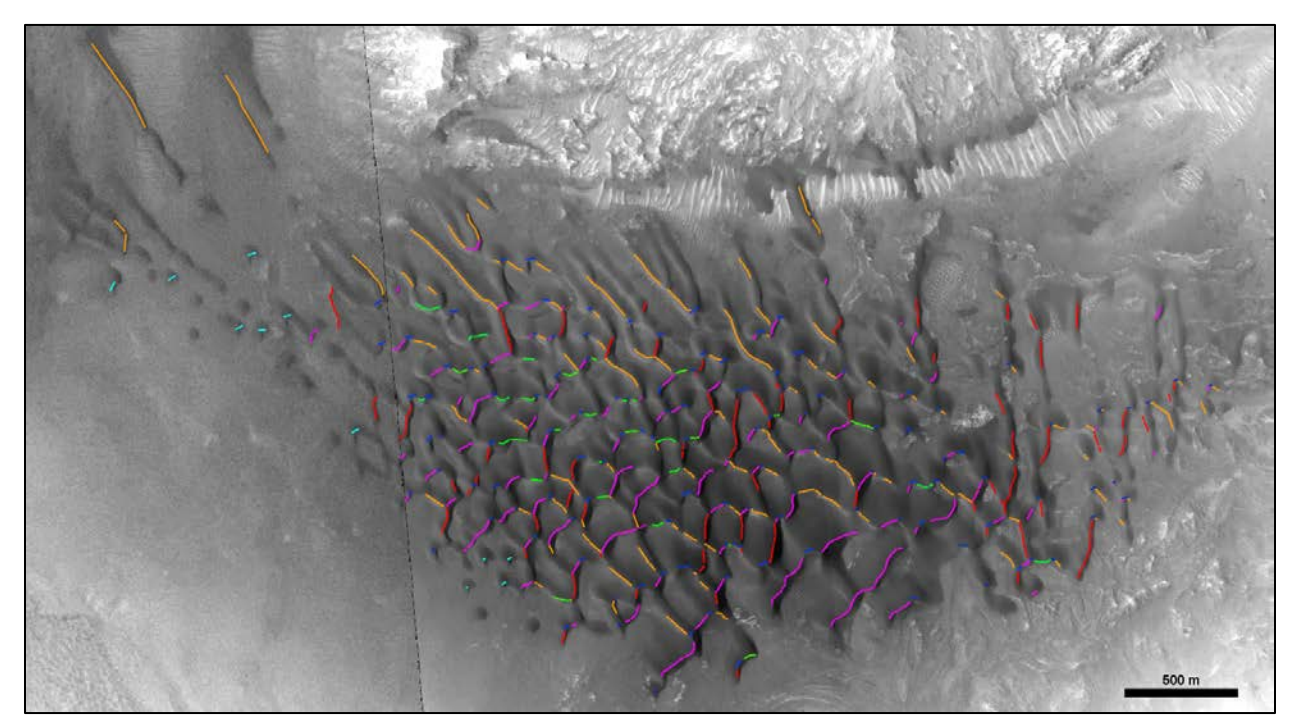


**Figure 10:** A composite image showing dune field NML030 from (L) CTX image F20\_043611\_2229\_XN\_42N031W and (R) HiRISE image ESP\_043611\_2230 with colored crestline measurements overlaid.

Using the grouped crestlines and the identified dune morphologies, the light blue, dark blue, pink, and green crestline groups were determined to be in bed instability mode and therefore suitable for use with the IMGBNT inferred wind direction method. The light blue crestlines are type II measurements which identify individual barchan dunes located in the northwest corner of NML030 and move towards the southeast. These type II measurements also provide the initial inferred wind direction of 329.2°. IMGBNT calculations using the initial inferred wind direction and the bedform trends of the pink and green crestline groups were calculated resulting in the output of Figure 11a and 11b. The mean trending direction of the pink group crestlines were calculated to be 45.1°. Figure 11a shows the range of possible wind directions that are capable of creating transverse dunes. The initial inferred wind direction falls well within this possible range and has been interpreted to be the primary wind direction that most recently shaped the pink group crestlines. Figure 11b shows the range of wind directions and does not include the primary wind direction determined for the light blue and pink crestline sets. Based on the quantity of green crestlines and their measured lengths, the wind direction that most recently altered them should have a transport ratio of approximately 1:4 to the initial wind direction which would equate to a secondary inferred wind direction of ~25°+/- 34°.

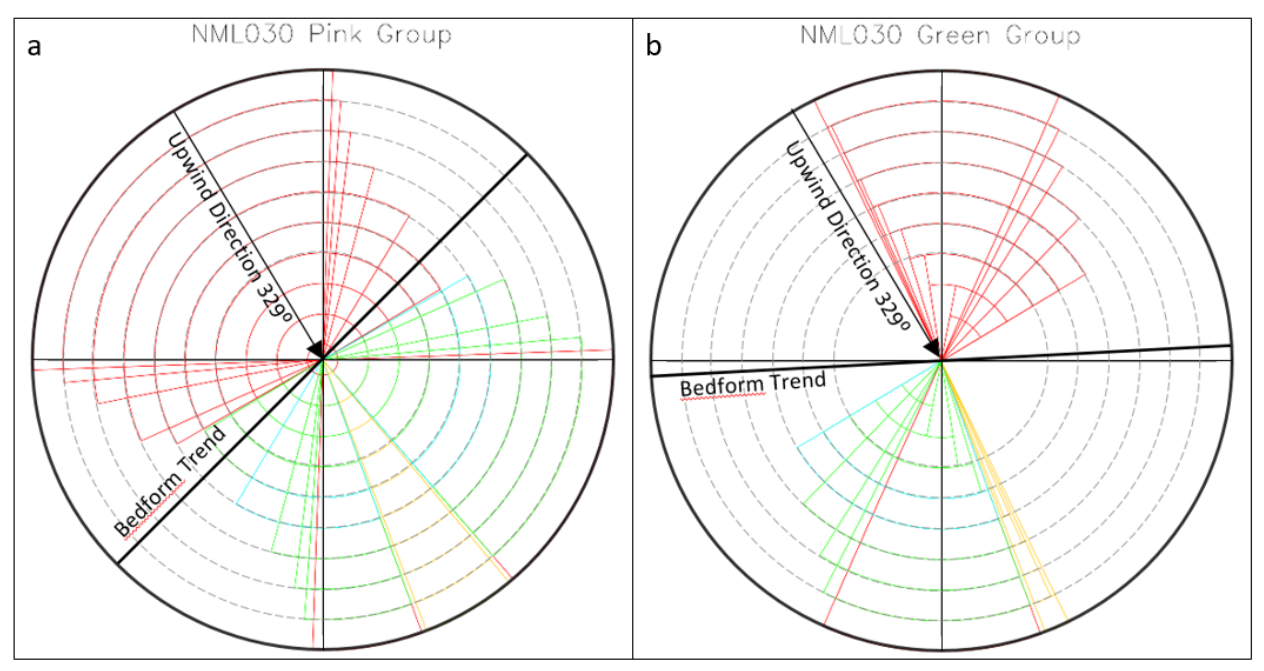


Figure 11: Results from IMGBNT calculations for dune field NML030.

### **5.2 Dune Field NML063 Inferred Wind Directions**

To the west of NML030 is NML063, the smallest dune field in TR4 located at 43.4 N and 319.3 E. This field contains 58 crestlines that were separated into 4 groups: dark blue (Type II), green (Type I), orange (Type I), and red (Type I). Figure 12 shows a portion of HiRISE image ESP\_019124\_2240 that covers NML063 and the colored crestline groups. Barchanoid dunes were the only morphology noted in this small field.

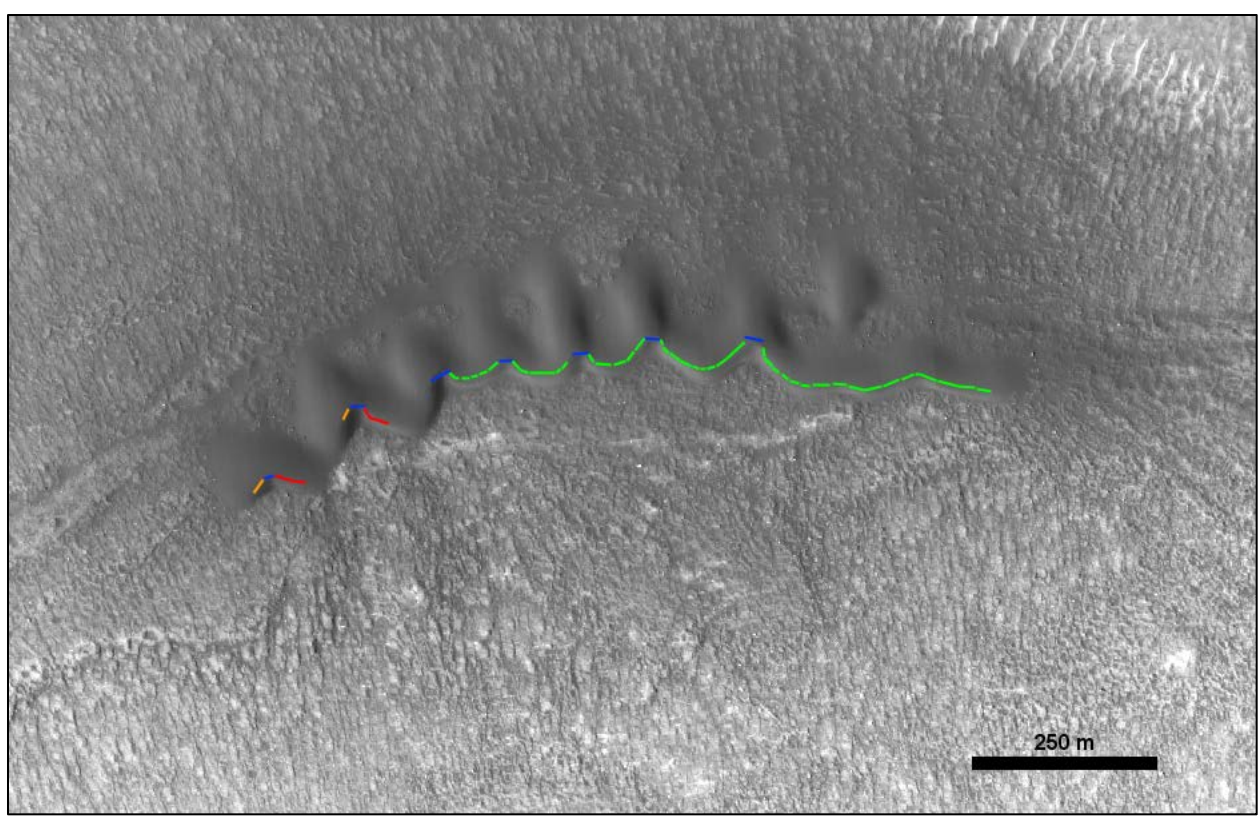
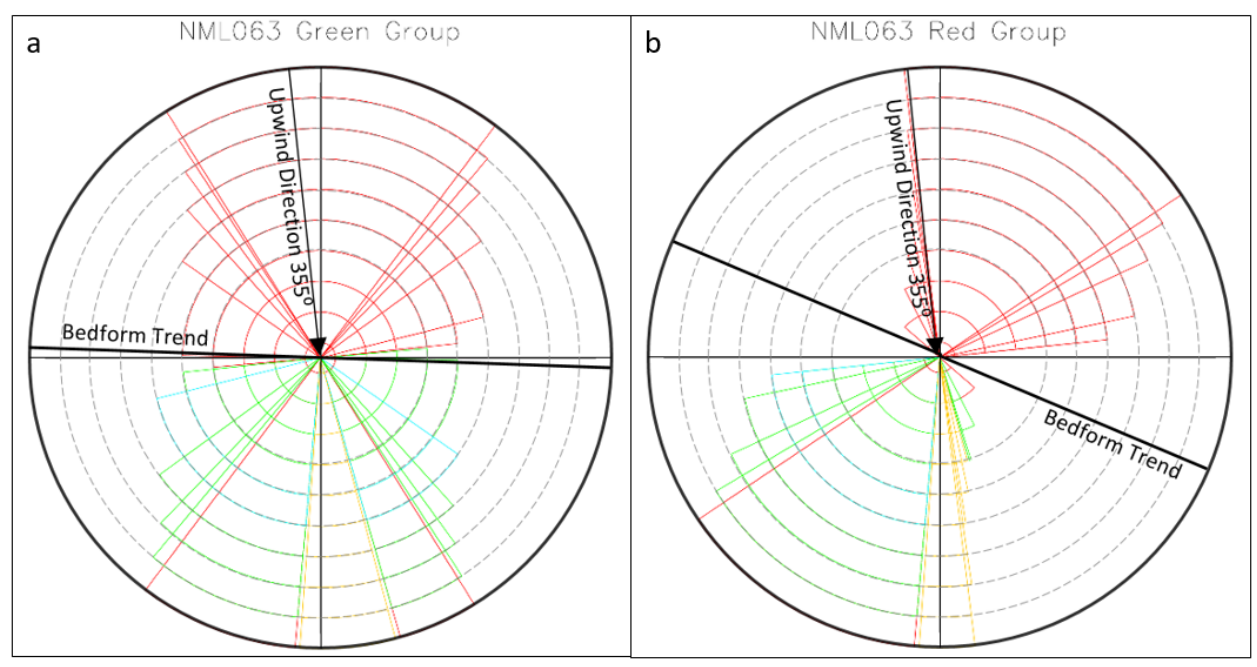


Figure 12: A view of dune field NML063 from HiRISE image ESP\_019124\_2240 with colored crestline measurements overlaid.

The barchanoid dunes in NML063 are aligned west to east indicating the primary wind direction is coming from the north and moving south. The dark blue crestlines are oriented in the same fashion and as type II measurements provide the primary inferred wind direction of 354.9°. Green and red crestline groups were chosen for IMGBNT calculation, the results of which are shown in Figure 13a and 13b. The green group crestlines trended at a mean value of 92°, nearly perpendicular to the initial inferred wind direction leading to the interpretation that the green crestlines were formed by the initial inferred wind direction. The red crestline group, although few in number, appear to have recorded a second wind direction. Crestlines for the red group trended in a mean direction of 113°. Due to the small size of the dune field and the lack of crestlines in the red group, the interaction of the initial inferred wind direction to this second inferred wind direction should favor the initial direction almost entirely leading to the interpretation that the transport ratio for the red group crestlines should be approximately 1:16 indicating a mean inferred wind direction of 22° +/- 62°.



**Figure 13:** Results from IMGBNT calculations for dune field NML063.

# **5.3 Dune Field NML040 Inferred Wind Directions**

To the southwest of NML063 is NML040, the second smallest dune field in TR4 located at 41.6 N and 314.1 E. 101 crestline measurements were made in this field and divided into 3 groups: dark blue (type II), pink (type I) and orange (type I). The colored crestlines are overlaid on HiRISE image PSP\_007257\_2220 and shown in Figure 14.

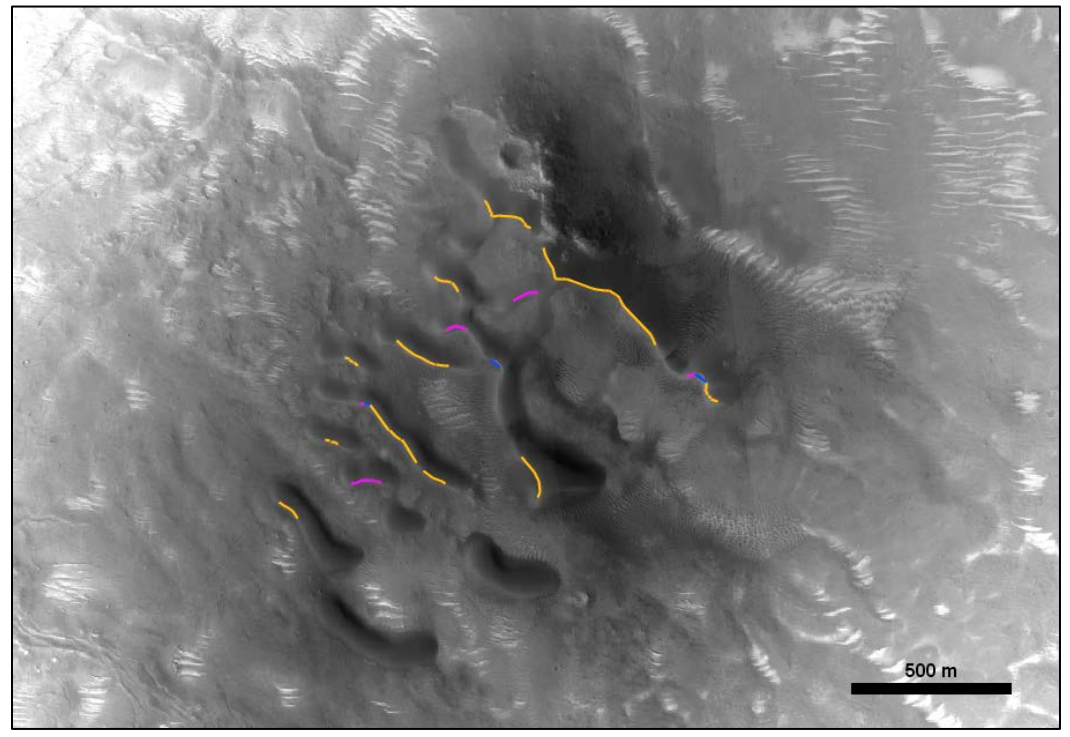


Figure 14: A view of dune field NML040 from HiRISE image PSP\_007257\_2220 with colored crestline measurements overlaid.

The set of dark blue crestlines are type II measurements which indicate an initial inferred wind direction of ~28°. Of the two remaining crestline groups, both appear to be in bed instability mode and were used for IMGBNT calculations. Results of the IMGBNT calculations for the orange and pink crestline groups are shown in Figure 15a and 15b. The orange group had a mean bedform trend direction of 130°, close to perpendicular to the initial inferred wind direction for this field. This led to the interpretation that the initial inferred wind direction has most recently influenced the crestline of the orange group. Results from the pink group IMGBNT calculation (Figure 15b) indicates that a second wind may be present. Due to the smaller number of pink to orange crestlines and the sizes of the pink crestlines, the estimated transport ratio between the initial inferred wind and a proposed second wind should be approximately 4:1. This transport ratio would make the second inferred mean wind direction 314° +/- 15°.

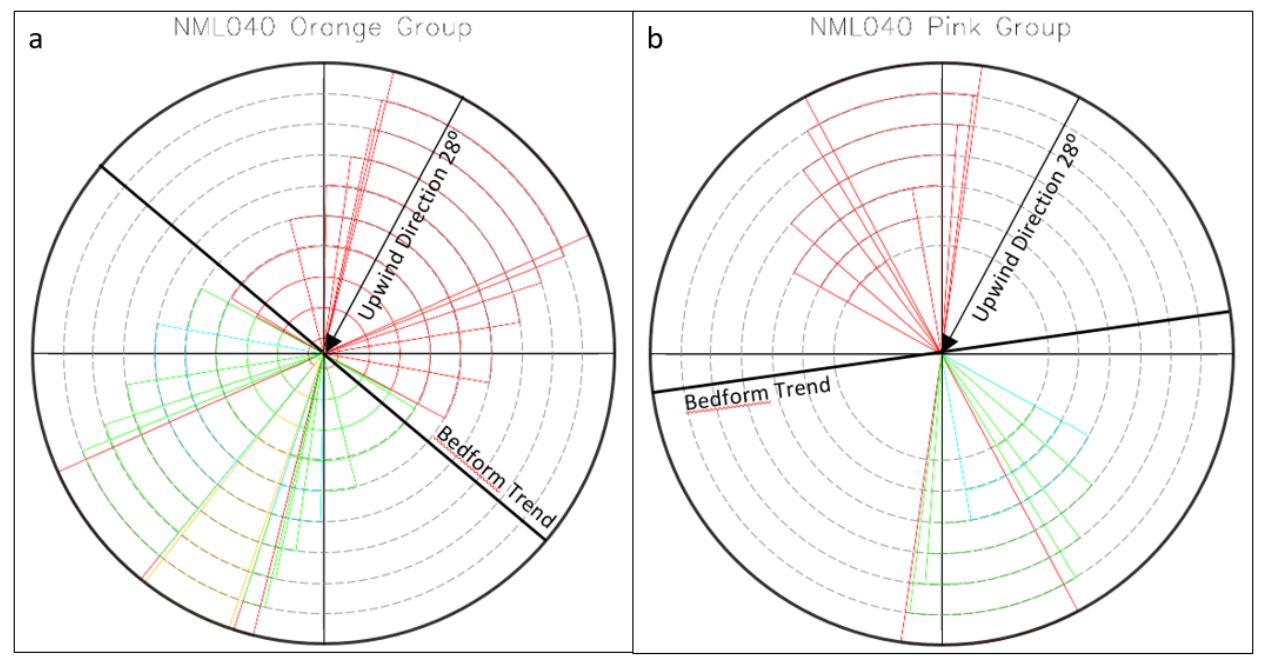


Figure 15: Results from IMGBNT calculations for dune field NML040.

### **5.4 Dune Field NML051 Inferred Wind Directions**

To the southeast of NML040 and south of NML030 is NML051 located at 36.5 N and 329.5 E. This is the third largest dune field of the five studied in TR4 and contains the most complex interpretation of wind patterns. A total of 453 crestlines were mapped in NML051 and seven groups were created: light blue (type II), blue (type II), dark blue (type II), orange (type I), pink (type I), green (type I), and red (type I). Figure 16 shows these groups of crestlines overlaid on HiRISE image ESP\_016737\_2170.

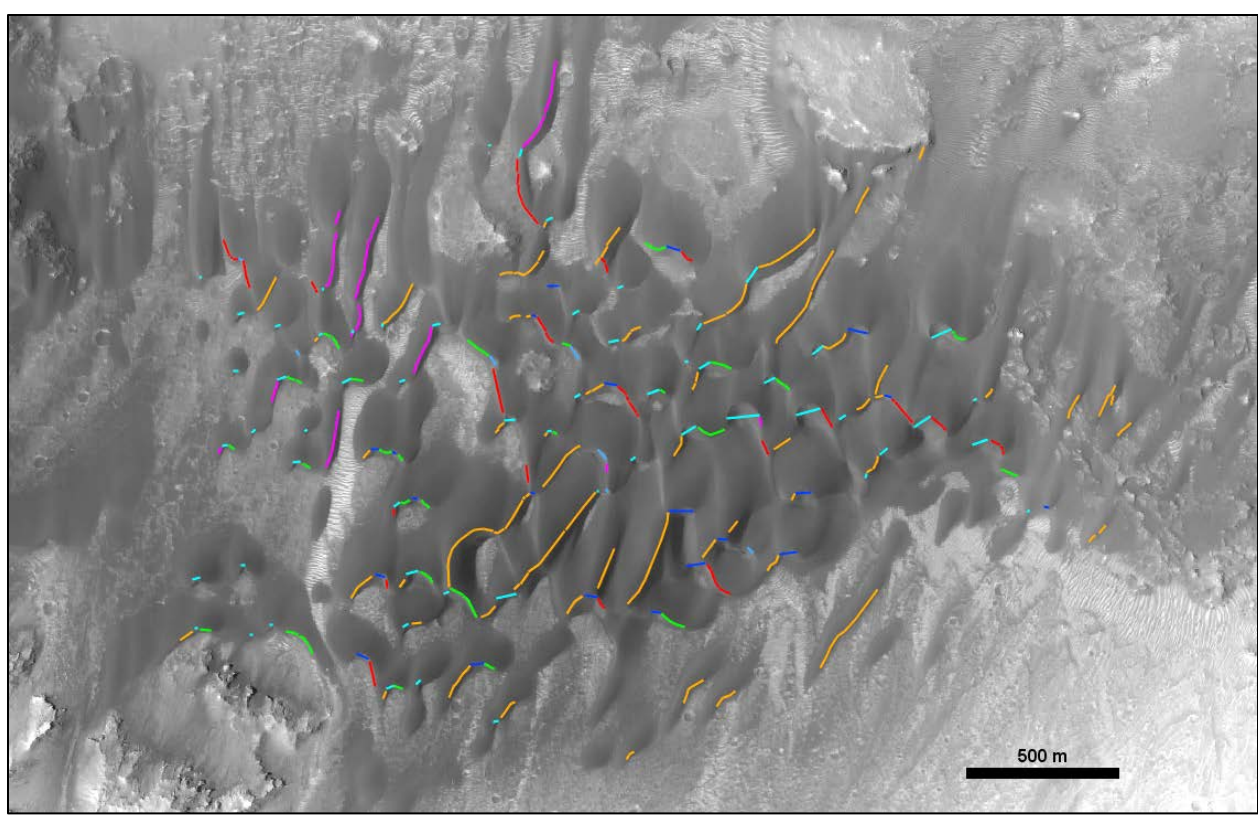


Figure 16: A view of dune field NML051 from HiRISE image ESP\_016737\_2170 with colored crestline measurements overlaid.

On the western side of NML051 small barchan dunes are visible with light blue, type II measurements. The light blue group was chosen to determine the initial inferred wind direction because it contained measurements of the only barchan dunes available in NML051. The light blue group indicated a mean initial inferred wind direction of 331.2°. Of the type I measurement groups, only the green and red groups appeared to be in bed instability mode and were used for IMGBNT calculations. The results of these calculations are shown in Figure 17a and 17b.

Green group crestlines had a mean bedform direction of 117.6° and red group crestlines had a mean bedform direction of 152.9°. Neither of these groups aligned as perpendicular or almost perpendicular indicating a second wind direction must a) be present and b) have a stronger impact on the crestlines (i.e. higher value in the transport ratio than the initial wind). Both ranges of possible wind directions capable of creating transverse dunes shown in Figure 17a and 17b overlap. Since IMGBNT can only provide two wind directions from calculations and the first direction was inferred to be 331.2, the second wind must be variable in wind direction and strength (i.e. transport ratio). Overlapping the ranges of possible winds from Figure 17a and 17b accounts for this variation and provides a range of inferred wind directions at three different transport ratios: 43°-54.5° at a transport ratio of 16:1, 47°-58.5° at 8:1, and 53°-63° at 4:1.

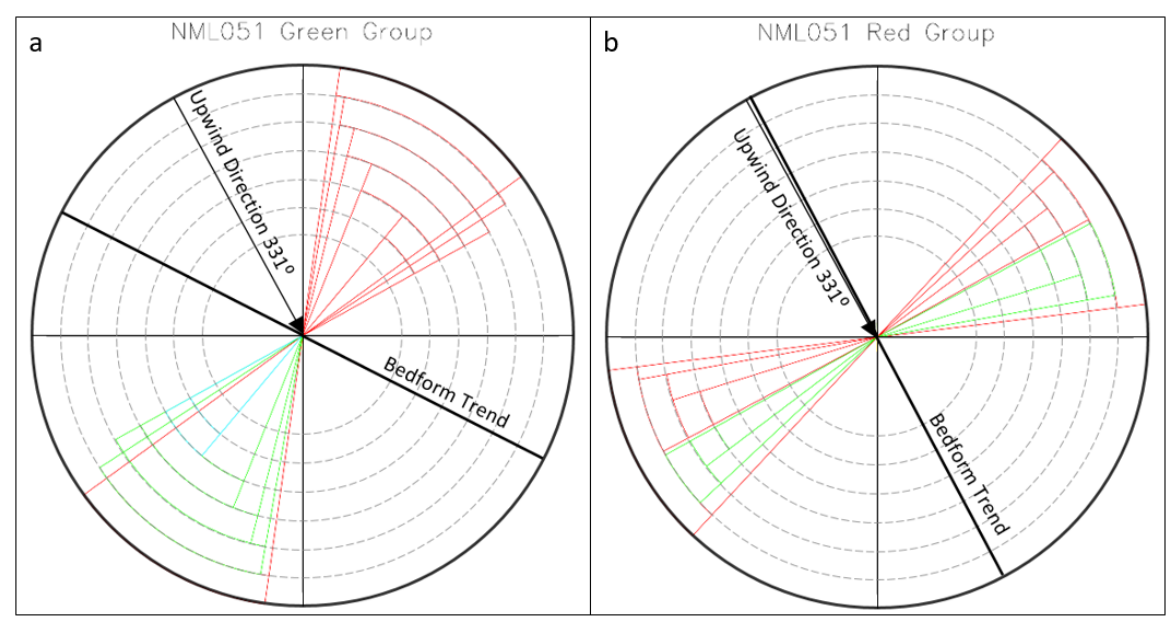
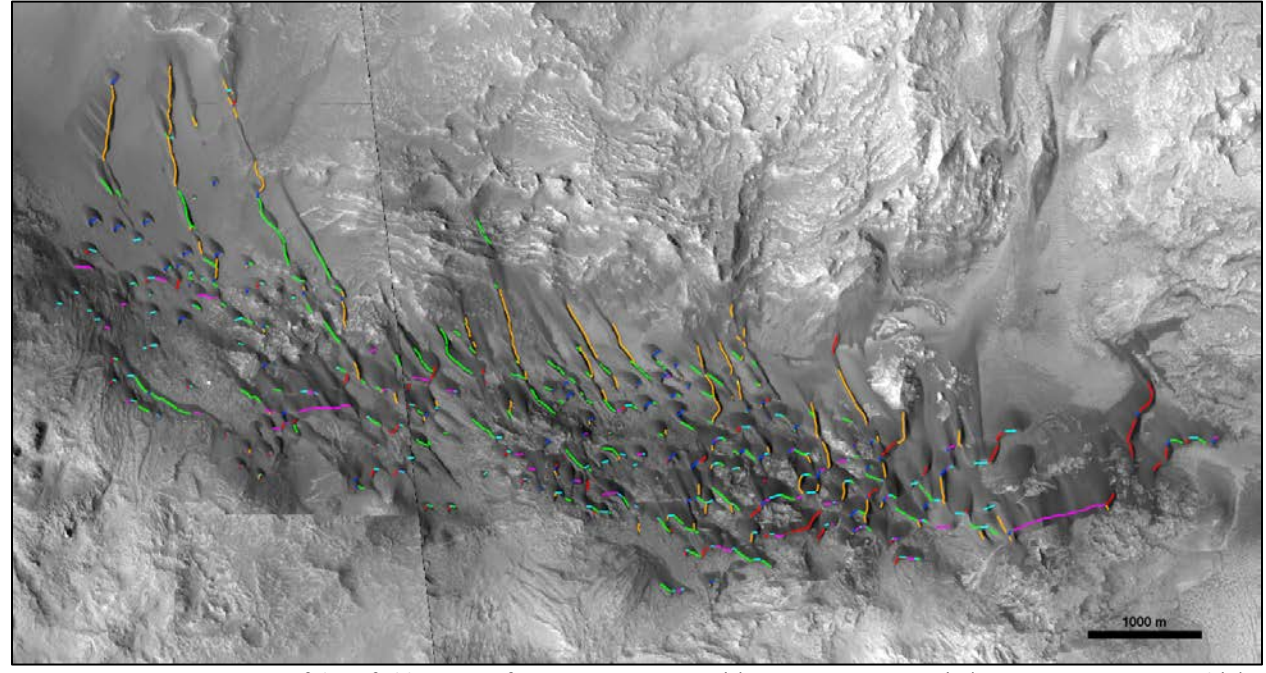


Figure 17: Results from IMGBNT calculations for dune field NML051.

### 5.5 Dune Field NML045

To the north of NML051 and just barely southeast of NML030 is NM045, located at 41.8 N and 329.6 E. This is the largest dune field in TR4 and the fifth dune field under investigation. A total of 1783 crestlines were mapped in this field and make up 6 groups of crestlines: dark blue (type II), light blue (type II), orange (type I), pink (type I), green (type I), and red (type I). A mosaic of HiRISE images (L) ESP\_054951\_2225, (M) ESP\_055373\_2220, and (R) ESP\_018372\_2225 show NML045 and the colored groups of crestlines in Figure 18.



**Figure 18:** A composite view of dune field NML045 from 3 HiRISE images (L) ESP\_054951\_2225, (M) ESP\_055373\_2220, and (R) ESP\_018372\_2225 with colored crestline measurements overlaid.

The western side of NML045 contains several particularly large barchan dunes which have type II measurements in the dark blue group. This group provides a mean initial inferred wind direction of 313.4°. Of the type I colored groups, the pink and red groups appear to be in bed instability mode and therefore capable of being used in IMGBNT calculations. Results of these calculations are displayed in Figure 19a and 19b. The red group had mean bedform direction of 32.3° which is nearly perpendicular to the initial inferred wind direction in this field. This led to the interpretation that the initial inferred wind direction has most recently shaped the crestlines in the red group. The pink group had a mean bedform trend direction of 85°. Results from the IMGBNT calculation in Figure 19b indicate a potential second inferred wind direction. Based on the number of crestline measurements in the pink group and the lengths of the measurements, the estimated transport ratio of the initial inferred wind to the second inferred wind is estimated to be approximately 4:1. This transport ratio would indicate the mean direction of the second inferred wind to be ~31.5° +/- 11.5°.

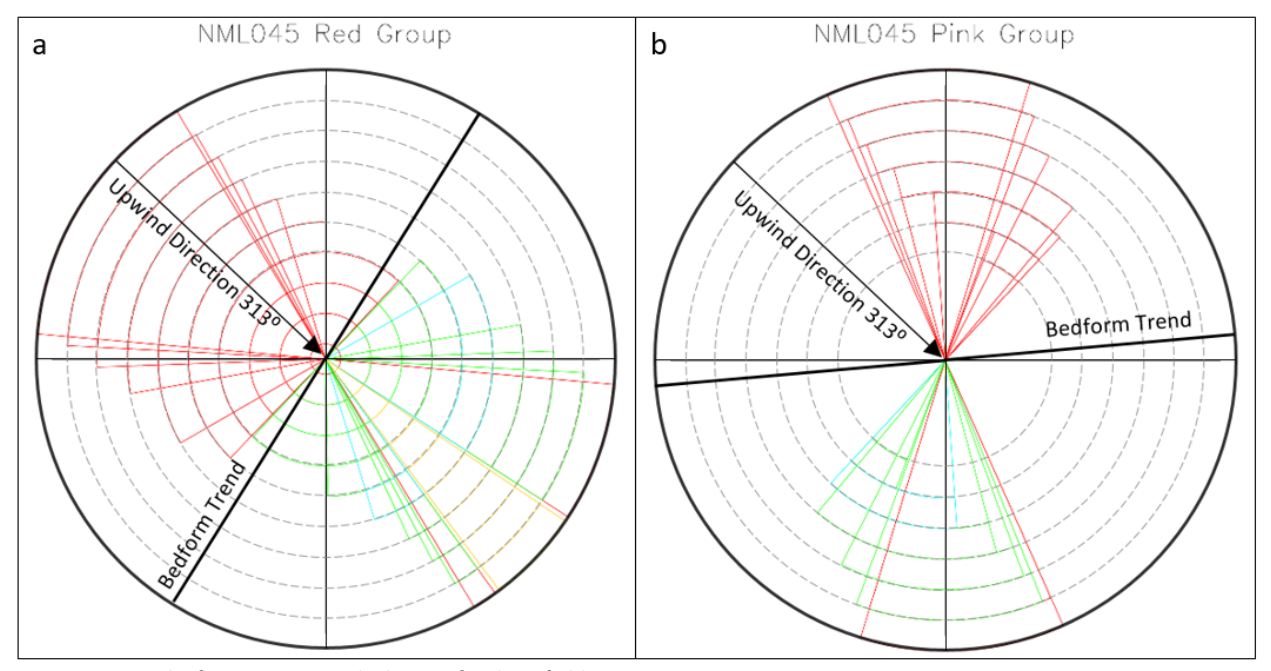
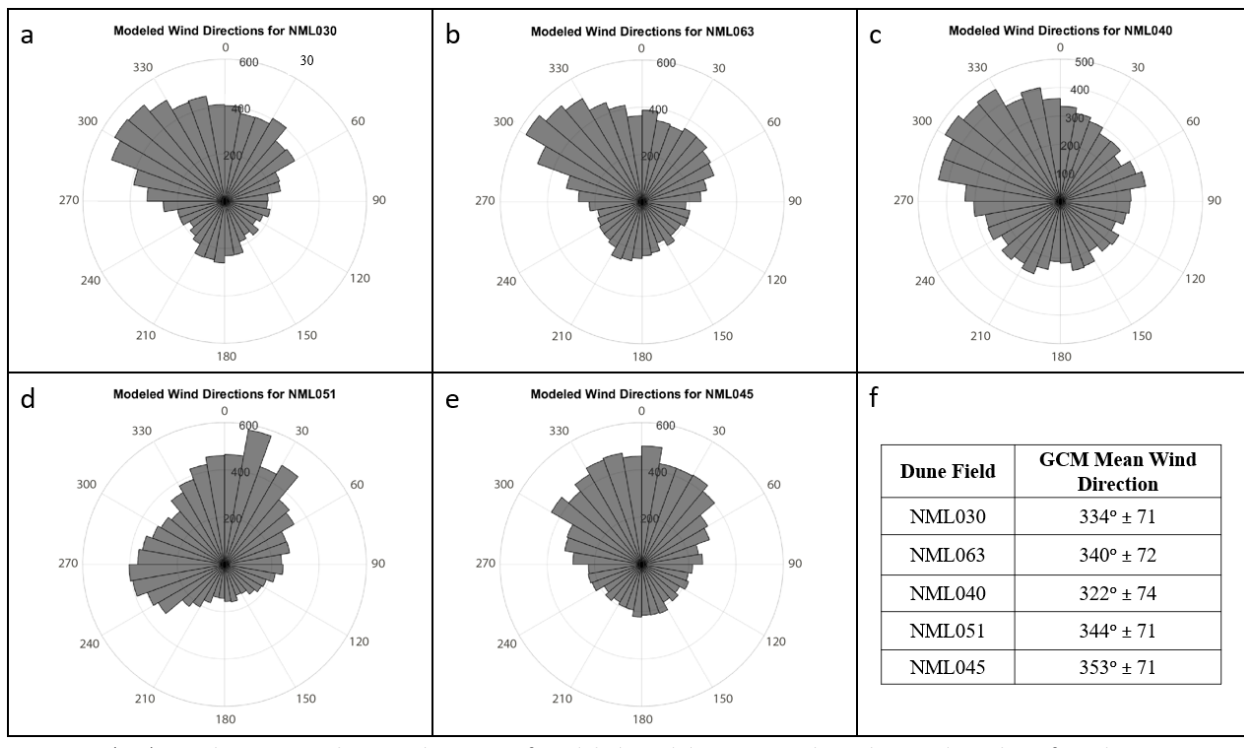


Figure 19: Results from IMGBNT calculations for dune field NML045.

# 5.6 GCM Results

Wind directions extracted from the NASA Ames GCM for Mars provides a second data set to compare with the inferred winds from each of the five dune fields in TR4. Figure 20a - 20e displays rose histograms of the upwind direction of the modeled winds from each model grid box covering TR4 that contained a dune field (shown in Figure 7). Each rose histogram contains 10,704 wind directions and span an entire Mars year. Figure 20f displays the mean modeled wind directions from each of the five dune fields in TR4.



**Figure 20:** (a-e) Rose histograms showing the range of modeled wind directions with 10° bins and number of wind measurements increasing as the bin moves away from the center of the histogram. (f) A table of mean wind directions and uncertainty values organized by dune field ID.

### **5.7 Statistical Tests**

A two sample, independent t-test was calculated for each pair of primary inferred and modeled winds for a total of 5 t-tests. Using a  $P_{crit}$  value of 0.2 for a 2-tailed test and values of degrees of freedom on the order of 10,000, a  $T_{crit}$  value of 1.282 was obtained. Based on the comparison of the calculated t values with the  $t_{crit}$  value, the null hypothesis was accepted in one of the five dune fields evaluated in this study. Table 2 displays the results of each t-test in relation to the  $t_{crit}$  value.

Dune Field	Calculated t Value	t_crit Value	Accept Null Hypothesis?
NML030	-1.169		Yes
NML063	3.022		No
NML040	-42.211	1.282	No
NML051	-4.378		No
NML045	-20.763		No

Table 2: Results of the t-tests calculated for each dune field study site.

# **5.8 Summary of Results**

Five dune fields in TR4 were analyzed with two methods to determine wind directions which shaped the dunes during the most recent period of dune construction. The first method inferred wind directions with high-resolution images of the martian surface and IMGBNT

calculations. This method of calculating inferred winds produces two wind directions, a primary and a secondary direction. The second method modeled wind directions over areas where the five dune fields are located. A t-test statistically compared the mean wind direction for the primary inferred wind and the modeled wind at each field. Of the five t-tests calculated, only one dune field (NML030) was found to have inferred winds that are not significantly different from the modeled winds. An overview of the results found in this study are shown in Table 3.

Dune Field	Primary Wind Direction (deg)	Secondary Wind Direction (deg)	Estimated Transport Ratio	GCM Wind Direction (deg)	GCM Matches Inferred Wind?
NML030	329 ± 14	$25 \pm 34$	4:1	$334 \pm 71$	Yes
NML063	$355 \pm 13$	$22 \pm 62$	16:1	$340 \pm 72$	No
NML040	$28 \pm 12$	$314 \pm 15$	4:1	$322 \pm 74$	No
		43-55	16:1		
NML051	331 ± 22	47-59	8:1	$344 \pm 71$	No
		53-63	4:1		
NML045	$313 \pm 16$	$32 \pm 12$	4:1	$353 \pm 71$	No

**Table 3:** Summary table showing all of the calculated results from inferred wind calculations, atmospheric modeling, and statistical testing.

### 6 DISCUSSION

# 6.1 Regional Interpretation of Wind Directions in TR4

Overall the primary inferred wind directions appear to be in close agreement with the modeled wind directions with the exception of NML040 although the secondary wind direction is much closer to the model prediction. Statistically, only the primary inferred wind direction at NML030 matches the GCM but if the  $P_{crit}$  value was decreased to 0.01 (meaning ~99% of the results are expected) NML063 would also match the winds modeled for that field and NML051 would not be far behind. Its also interesting that the means of the modeled winds appear to be consistent with one another when the grid boxes that were sampled were not adjacent except in one case. This would suggest that winds in the TR4 region move air preferentially from the northwest to the southeast.

#### 6.1.1 Potential Impact of Craters on Wind Directions

The five dune fields studied all exist in craters, three of which are simple craters with smooth floors and the remaining two are complex craters with an uplifted central mound. Although there was only one dune field where the mean inferred wind direction matched statistically with the model, the inferred winds at the other fields are consistent with one another making it difficult to determine how much the crater morphology affected the wind directions at each dune field. The same is true for the GCM results where there is no major deviation in any one grid box that could be linked to a crater. It should also be noted that most of the craters housing the dune fields for this study are small (see Table 1) and are not likely well resolved at the 5°x6° resolution of the GCM.

However, it was interesting to see that every dune field in this study had dunes showing morphologies consistent with at least two wind directions. The fields in the eastern portion of TR4 (NML030 in particular) provide good examples of this where the lines of barchans appear on the western side indicating winds flowing into the dune field from the northwest and moving southeast as well as some smaller dunes on the eastern side aligned in a northeast to south southwest trend. Many of the dunes aligned in this second direction through the eastern side of NML030, NML045, and NML051 appear to be in fingering mode and would therefore align with the direction of the wind. For NML030 in particular, a pair of nearly perpendicular winds, one entering from the northwest and the other from the northwest may make sense considering the host crater's central mound is adjacent to the north of NML030 so wind would have to flow around the mound to enter the field.

#### 6.1.2 Potential Environmental Patterns to Note

Part of the reason for choosing the five dune fields presented in this study was to compare characteristics of the dune fields against one another to search for patterns of characteristics among the fields. Dune fields NML030, NML045, and NML051 essentially fall in a vertical line on the eastern side of TR4 (see Figure X) while NML063 and NML040 are located in similar longitudes and west of the first three fields. An apparent trend present in the studied dune fields is the constraint on sand moving from east to west across TR4. NML030, NML045, and NML051 all have considerable sizes for mid-latitude dune fields however, NML063 and NML040 are much smaller. Two possible interpretations for this could be: 1) the eastern portion of TR4 is much closer to a source of sediment that has created the dune fields in question or 2) wind strengths decrease significantly as they move westward through the target region reducing the amount of sediment being supplied to NML063 and NML040.

Another potential pattern to note involves the three fields on the eastern side of TR4. In all three field near the western edge of each dune field are groups of barchan dunes that appear aligned from the northwest to the southeast. This is particularly interesting given that the types of craters vary between simple and complex among the three fields (meaning the addition of a central mound that air has to flow over or around to reach the dune field) and that the craters have different diameters but are thought to have an affect on the winds.

# **6.2 Influence of Statistics in Comparing Wind Directions**

The use of statistics in this study plays a major role in deciding how similar the directions of the primary inferred winds are to the modeled winds. However, inconsistencies in the statistical approach may have skewed the results. A t-test works on several assumptions including a normal distribution of data for each sample, datasets are collected independently of one another, data is randomly sampled, and variance between sample sizes is small. As previously mentioned in the methods section, the modeled data may have had a slightly non-normal distribution causing an inconsistency in the t-tests. Additionally, the variation in sample sizes between the type II measurements and the output from the model was considerate and may have also caused some statistical inconsistencies.

A potential fix for these problems would be to explore some non-parametric tests for future iterations of this work, tests specifically designed for non-normal distributions of data. Variations in sample sizes between the total number of points obtained and the number of data points used in calculations may also help represent a more accurate method of comparing inferred and modeled wind directions.

### 7 ACKNOWLEDGEMENTS

I would like to thank Dr. Phillip Piccoli and Dr. Serinia Diniega for their comments regarding the development of various pieces of this project's methodology. University of Maryland's Geology and Astronomy Departments were particularly helpful in providing faculty feedback from project updates and lending the use of several computer resources, respectively. The use of the JMARS software was crucial to the development of this project and I'd like to thank the entire JMARS team for their help as well as the HiRISE and CTX science teams for continuing to provide high quality datasets for public use.

#### 8 REFERENCES

Berens, P., 2009. CircStat: A matlab toolbox for circular statistics. Journal of Statistical Software. 31. 1-21.

Bridges, N.T., Ayoub, F., Avouac, J.-P., Leprince, S., Lucas, A., Mattson, S., 2012. Earth-like sand fluxes on Mars. Nature. 485, 339–342.

Christensen, P. R., Engle, E., Anwar, S., Dickenshied, S., Noss, D., Gorelick, N., & Weiss-Malik, M. (2009) JMARS—A planetary GIS. Paper presented at the American Geophysical Union Fall Meeting, San Francisco, CA, Abstract IN22A-06.

Diniega, S., Kreslavsky, M., Radebaugh, J., Silvestro, S., Telfer, M., Tirsch, D., 2017. Our evolving understanding of aeolian bedforms, based on observation of dunes on different worlds. Aeolian Research, Special Issue for the Fourth International Planetary Dunes Workshop. 26, 5–27.

Fenton, L.K., Hayward, R.K., 2010. Southern high latitude dune fields on Mars: Morphology, aeolian inactivity, and climate change. Geomorphology. 121, 98–121.

Fenton, L.K., Michaels, T.I., Beyer, R.A., 2014a. Inverse maximum gross bedform-normal transport 1: How to determine a dune-constructing wind regime using only imagery. Icarus. 230, 5-14.

Fenton, L.K., Michaels, T.I., Chojnacki, M., Beyer, R.A., 2014b. Inverse maximum gross bedform-normal transport 2: Application to a dune field in Ganges Chasma, Mars and comparison with HiRISE repeat imagery and MRAMS. Icarus. 230, 47-63.

Fenton, L.K., Carson, C.C., Michaels, T.I., 2018. Climate forcing of ripple migration and crest alignment in the last 400 kyr in Meridiani Planum, Mars. J. Geophys. Res. 123, 849-863.

Gardin, E., Allemand, P., Quantin, C., Silvestro, S., Delacourt, C., 2012. Dune fields on Mars: Recorders of climate change?. Planetary and Space Science. 60, 314-321.

Hayward, R.K., Mullins, K.F., Fenton, L.K., Hare, T.M., Titus, T.N., Bourke, M.C., Colaprete, A., Christensen, P.R., 2007a. Mars Global Digital Dune Database and initial science results. J. Geophys. Res. 112, E11007. doi:10.1029/2007JE002943.

Hayward, R.K., Titus, T.N., Michaels, T.I., Fenton, L.K., Colaprete, A., Christensen, P.R., 2009. Aeolian dunes as ground truth for atmospheric modeling on Mars. J. Geophys. Res. 114, E11012. doi: 10.1029/2009JE003428.

Hayward, R.K., Fenton, L.K., Titus, T.N., 2014. Mars Global Digital Dune Database (MGD3): Global dune distribution and wind pattern observations. Icarus. 230, 38-46.

Kahre, M.A., Murphy, J.R., Haberle, R.M., 2006. Modeling the Martian dust cycle and surface dust reservoirs with the NASA Ames general circulation model. J. Geophys. Res. 111, E06008. doi:10.1029/2005JE002588

Malin, M.C., Bell, J.F., Cantor, B.A., Caplinger, M.A., Calvin, W.M., Clancy, R.T., Edgett, K.S., Edwards, L., Haberle, R.M., James, P.B., Lee, S.W., Ravine, M.A., Thomas, P.C., Wolff, M.J., 2007. Context Camera Investigation on board the Mars Reconnaissance Orbiter. J. Geophys. Res. 112, E05S04. doi:10.1029/2006JE002808.

McEwen, A.S., Eliason, E.M., Bergstrom, J.W., Bridges, N.T., Hansen, C.J., Delamere, W.A., Grant, J.A., Gulick, V.A., Herkenhoff, K.E., Keszthelyi, L., Kirk, R.L., Mellon, M.T., Squyres, S.W., Thomas, N., Weitz, C.M., 2007. Mars Reconnaissance Orbiter's High Resolution Imaging Science Experiment (HiRISE). J. Geophys. Res. 112, E05S02. doi:10.1029/2007JE002605.

McKee, E.D., 1979. Introduction to a study of global sand seas. In: McKee, E.D. (Ed.), U.S. Geol. Surv. Prof. Pap, 1052, pp. 3-17.

Pont, S.C. du, Narteau, C., Gao, X., 2014. Two modes for dune orientation. Geology. 42, 743–746.

Reffet, E., Pont, S.C. du, Hersen, P., Douady, S., 2010. Formation and stability of transverse and longitudinal sand dunes. Geology. 38, 491–494.

Robbins, S.J., Hynek, B.M., 2012a. A new global database of Mars impact craters ≥1 km: 1. Database creation, properties, and parameters. J. Geophys. Res. 117, E05004. doi:10.1029/2011JE003966

Rubin, D.M., Hunter, R.E., 1987. Bedform Alignment in Directionally Varying Flows. Science. 237, 276–278.

Rubin, D.M., Ikeda, H., 1990. Flume experiments on the alignment of transverse, oblique, and longitudinal dunes in directionally varying flows. Sedimentology. 37, 673–684.

Tanaka, K.L., Skinner, J.A., Jr., Dohm, J.M., Irwin, R.P., III, Kolb, E.J., Fortezzo, C.M., Platz, T., Michael, G.G., and Hare, T.M., 2014. Geologic map of Mars: U.S. Geological Survey Scientific Investigations Map 3292. scale 1:20,000,000, pamphlet 43

Widmer, J.M., Diniega, S., 2018. New alcove activity in Lyot crater: A modern-day mystery in the martian mid latitudes. Lunar Planet. Sci. XLIX. 1651-1652 (abstract).

Widmer, J.M., Diniega, S., 2019. Constraining the spatial extent and timing of local-scale seasonal frost in the northern mid-latitude region of Mars. Lunar Planet. Sci. L. 1990-1991 (abstract).

Zurek, R.W., Smrekar, S.E., 2007. An overview of the Mars Reconnaissance Orbitor (MRO) science mission. J. Geophys. Res. 112, E05S01. doi:10.1029/2006JE002701